Neurochemical and Structural Organization of the Principal Nucleus of the Inferior Olive in the Human

JOAN S. BAIZER,[1]* CHET C. SHERWOOD,[2] PATRICK R. HOF,[3] SANDRA F. WITELSON,[4] AND FAHAD SULTAN[5]

[1]Department of Physiology and Biophysics, University at Buffalo, Buffalo, New York
[2]Department of Anthropology, The George Washington University, Washington, District of Columbia
[3]Department of Neuroscience and Friedman Brain Institute, Mount Sinai School of Medicine, New York, New York
[4]Department of Psychiatry & Behavioural Neurosciences, Michael G. DeGroote School of Medicine, McMaster University, Hamilton, Ontario, Canada L8N 3Z5
[5]Department of Cognitive Neurology, University of Tübingen, Tübingen, Germany

ABSTRACT

The inferior olive (IO) is the sole source of the climbing fibers that innervate the Purkinje cells of the cerebellar cortex. The IO comprises several subdivisions, the dorsal accessory olive (DAO), medial accessory olive (MAO), and principal nuclei of the IO (IOpr); the relative sizes of these subnuclei vary among species. In human, there is an expansion of the cerebellar hemispheres and a corresponding expansion of the IOpr. We have examined the structural and neurochemical organization of the human IOpr, using sections stained with cresyl violet (CV) or immunostained for the calcium-binding proteins calbindin (CB), calretinin (CR), and parvalbumin (PV), the synthetic enzyme for nitric oxide (nNOS), and nonphosphorylated neurofilament protein (NPNFP). We found qualitative differences in the folding patterns of the IOpr among individuals and between the two sides of the brainstem. Quantification of IOpr volumes and indices of folding complexity, however, did not reveal consistent left–right differences in either parameter. Single-label immunohistochemistry showed that populations of neurons in the IOpr express CB, CR, NPNFP, and nNOS. Individual fibers labeled for PV, CB, CR, NPNFP, and nNOS were also found. There was individual variability in the numbers and density of stained neurons in the human IOpr; such variability was not seen in other brainstem nuclei. These data are consistent with, and complement, earlier studies showing a dramatic age-related increase in lipofuscin and decrease in RNA in the human IOpr. The impact of these changes in the IOpr on cerebellar function is, however, not known. Anat Rec, 294:1198–1216, 2011. © 2011 Wiley-Liss, Inc.

Key words: cerebellum; climbing fibers; cerebral cortex

Additional Supporting Information may be found in the online version of this article.

Grant sponsor: Department of Physiology and Biophysics, University at Buffalo; Grant sponsor: James S. McDonnell Foundation; Grant number: 22002078.

*Correspondence to: Joan S. Baizer, Department of Physiology and Biophysics, 123 Sherman Hall, University at Buffalo, Buffalo, NY 14214. Fax: +1-716-829-3096. E-mail: baizer@buffalo.edu

Received 7 March 2011; Accepted 28 March 2011
DOI 10.1002/ar.21400
Published online 31 May 2011 in Wiley Online Library (wileyonlinelibrary.com).

The inferior olive (IO) is the only source of climbing fibers that innervate Purkinje cells of the cerebellar cortex (Armstrong, 1974; Voogd et al., 1990) and is present in all vertebrates that have a cerebellum (see Kooy, 1917, for the classic description of the structure of the IO in different species). The IO consists of three major subdivisions, the dorsal accessory olive (DAO) and medial accessory olive (MAO), and the principal nucleus of the IO (IOpr; Paxinos et al., 1990; Voogd et al., 1990). Different subdivisions project to different regions of the cerebellum, the DAO to the anterior lobe, the MOA to the flocculus and vermis (Voogd et al., 1990), and the IOpr to the cerebellar hemispheres (Armstrong, 1974; Azizi and Woodward, 1987; Voogd et al., 1990). There are major species differences in the size of the different IO nuclei (Kooy, 1917; Armstrong, 1974; Azizi and Woodward, 1987). These differences parallel differences in the development of the cerebral cortex and the cerebellum. In great apes and humans, there is a dramatic expansion of the cerebral cortex and a parallel enlargement of the cerebellar hemispheres and dentate nucleus (Matano and Hirasaki, 1997; Matano and Ohta, 1999; MacLeod et al., 2003; Sultan and Glickstein, 2007; Sherwood et al., 2008; Glickstein et al., 2009; Balsters et al., 2010; Sultan et al., 2010). There is a corresponding dramatic expansion of the IOpr.

In the present study, we addressed several questions about the structural and neurochemical organization of the human IOpr. First, we have previously found that immunoreactivity to calcium-binding proteins and other markers could reveal subdivisions in brainstem structures of several species (Baizer and Baker, 2005; Baizer and Baker, 2006a, 2006b; Baizer and Broussard, 2010); and we sought to determine whether the human IOpr might have similar subdivisions. This idea was prompted by the relationship of the IOpr with the cerebellar hemispheres and dentate nucleus, as functional and neurochemical subdivisions of the dentate nucleus have been found in primates (Dum et al., 2002). We also asked if there might be neurochemical heterogeneity of the neurons of the IOpr as seen in their projection targets, the Purkinje cells (Brochu et al., 1990). Finally, we investigated whether the structure of the IOpr mirrors the structural and functional asymmetries of the cerebral cortex related to handedness and language (Toga and Thompson, 2003).

Our results show individual differences in the size, shape, and folding pattern of the IOpr, as well as asymmetry in that folding pattern in any given individual, but no evidence for population-level left–right differences in IOpr volume or folding complexity. An unexpected, but dramatic, finding was marked differences among cases in the numbers of neurons in the IOpr that were immunostained for the markers we tested.

Some of these data have been presented previously in abstracts (Baizer and Baker, 2006a; Baizer et al., 2007a; Baker et al., 2007).

MATERIALS AND METHODS

Tissue Preparation

For immunohistochemistry, we used seven human brainstems from the Witelson Normal Brain Collection (Witelson and McCulloch, 1991; Table 1, Cases 1–7). All these cases were right-handed. The history of the tissue and the methods of histology and immunohistochemistry have been described previously (Baizer et al., 2007b; Baizer and Broussard, 2010). Briefly, tissue blocks were oriented on a custom-built freezing stage of an American Optical sliding microtome in the transverse plane; the blocks were placed as symmetrically as possible. Forty micrometer thick frozen sections were cut and stored at 4°C in 5% formalin in plastic compartment boxes, five sections/compartment. Sections about 1 mm apart from each case were mounted on gelled slides and stained with cresyl violet (CV); more closely spaced sections were stained and used to determine the rostral and caudal limits of the IOpr.

We also sectioned and stained an additional four brainstem samples including the IO from younger cases obtained from the Brain Bank of the Mount Sinai School of Medicine, NY. For the three-dimensional (3D) reconstruction of the IOpr, we used sections from an additional case that had been a neurosurgical patient (Barrow Neurological Institute, Phoenix, AZ). The brain was removed and immersion fixed in 10% formalin and frozen sections of the brainstem made in the parasagittal plane (example shown in Supporting Information

TABLE 1. Cases and tissue history

Case		Source	Age	Gender	PMI	Cause of death	Year
1	155	W	50	W	9	Breast cancer	1988
2	158	W	51	M	1	Colorectal cancer	1989
3	164	W	45	W	3	Breast cancer	1991
4	168	W	69	M	3	Rectal cancer	1992
5	169	W	70	M	2	Colorectal cancer	1992
6	176	W	71	W	3	Colon cancer	1994
7	180	W	54	M	2	Adenocarcinoma	1995
8	1,342	MSSM	36	M	17	Anaphylaxis	2006
9	1,130	MSSM	38	M	24	Accident	2004
10	1,057	MSSM	40	W	4	Aortic dissection	2003
11	1,319	MSSM	48	M	17	Aortic stenosis	2006
12	98–99	GVA	75	W	10	Bronchopneumonia	1999
13	60–01	GVA	79	M	28	Cardiac failure	2001
14	33–02	GVA	77	W	8	Myocardiac infarct	2002
15	AG-1	BNI					

W, Witelson Normal Brain Collection; MSSM, Mount Sinai School of Medicine Brain Bank; GVA, University of Geneva School of Medicine Human Brain Collection; and BNI, Barrow Neurological Institute.

TABLE 2. Primary antibodies

Antigen	Immunogen	Manufacturer, species, type, catalogue number	Dilution	Visualization
Calbindin D28	Recombinant calbindin	Chemicon, rabbit polyclonal, #AB1778	1:1,000–1:2,000	DAB/GO, IF
Calretinin	Recombinant rat calretinin	Chemicon, rabbit polyclonal, #AB5054	1:2,000–1:3,000	DAB/GO
Calretinin	Guinea pig calretinin	Chemicon, goat polyclonal, #AB1550	1:250	IF
GAD65/67	Synthetic peptide sequence DFLIEEIERLCDQDI from the C-terminus of glutamate decarboxylase (GAD)	Serotec, rabbit polyclonal, #AHP360	1:200	DAB/GO
nNOS	Amino acids 1,422–1,433, human nNOS	Cayman, rabbit polyclonal, #160870	1:200	DAB/GO
Parvalbumin (PV)	Purified frog muscle PV	Sigma, mouse monoclonal, #P-3171	1:2,000	DAB/GO
Neurofilament H-nonphosphorylated	Nonphosphorylated mammalian neurofilament H	Sternberger monoclonals/Covance	1:1,000–1:3,000	DAB/GO

Fig. 1). Sections were stained with CV and the slides scanned with a CCD camera at an *x–y* resolution of 0.025 mm (Nikon DXM100). To make the 3D models, 26 sections 280 μm apart were aligned with Amira software (Amira 4.1.1, Mercury Computer Systems, Chelmsford). Following alignment, the sections' stack was reassembled to an *x–y–z* resolution of 0.04 × 0.04 × 0.14 mm^3 and by Lanczos resampling. The contours of the IO were traced manually and smoothed with a Gaussian filter (kernel size 5 × 5 × 5 and relative sigma of 0.6 × 0.6 × 0.6). A 3D surface model was generated by triangulation with Amira software. The contours of the IO were traced and the 3D surface models and the movie showing the IOpr rotating in 3D (see Supporting Information figures) were also made with Amira software. Table 1 summarizes all the human cases used.

In addition to the human material, we also used archival slides and sections from rat, rhesus monkey, and cat, sections from a common chimpanzee brainstem (female, age 45) that were cut and processed for this study, and archival sections of five additional chimpanzees (3 males, 2 females, mean age = 24 years), four Western lowland gorillas (2 males, 2 females, mean age = 35 years), and four Bornean orangutan (2 males, 2 females, mean age = 35 years) brainstems that had been stained with CV.

Antibody Characterization

Table 2 shows the primary antibodies and dilutions used. For all antibodies, no immunostaining was seen on control sections on which the primary antiserum was omitted.

The calbindin D28 (CB) antiserum (AB1778, Chemicon, Temecula, CA) was affinity purified and preabsorbed against calretinin (CR). It recognizes a band of 28 kDa on a Western blots of mouse brain (manufacturer's data sheet). No immunostaining was seen on control sections in which the antiserum was diluted (1:2,000) and incubated with the protein (Swant, recombinant rat calbindin, 2 μg/ml, in 1 ml antibody diluent) for 6 hr at 4° C before immunostaining [following the Swant (Bellinzona, Switzerland) protocol].

The first CR antiserum (AB5054, Chemicon) recognizes a band of 31 kDa on Western blots of rat brain (manufacturer's data sheet). No immunostaining was seen on control sections in which the antiserum was diluted (1:1500 in 1.5 ml of antibody diluent) and preincubated with the CR protein (Swant, recombinant human CR produced in *Escherichia coli*, 3 μg/ml) for 6 hr at 4°C before immunostaining (following Swant instructions). The second CR antiserum (AB1559, Chemicon) was used for double-label immunofluorescence and resulted in staining in the IOpr identical to that seen with AB5054.

The GAD65/67 antiserum (SEROTEC, Oxford, UK) recognizes both molecular isoforms of glutamic acid decarboxylase, GAD65 and GAD67 with bands of 65 and 67 kDa on Western blots of rat brain lysate (manufacturer's data sheet). The nitric oxide synthase (nNOS) antiserum (Cayman Chemical, Ann Arbor, MI) recognized a peptide of 155 kDa on Western blots of mouse brain (manufacturer's quality control sheet). No immunostaining was seen on control sections in which the antibody was first incubated with the immunizing protein (Cayman Chemical, Catalogue 360871, 1 μg/ml) for 1 hr at RT before dilution (1:200 in 2 cc of antibody diluent; following Cayman instructions) and immunostaining.

The neurofilament H antiserum recognizes only nonphosphorylated epitopes (nonphosphorylated neurofilament protein, abbreviated NPNFP, also abbreviated SMI-32; Covance, Emeryville, CA and Sternberger Monoclonals, Baltimore, MD) on the medium (170 kDa) and heavy (200 kDa) molecular weight subunits of neurofilament H in immunoblots of mammalian brainstem and spinal cord tissue (described in Sternberger and Sternberger, 1983; Lee et al., 1988; Ingham et al., 2009 and in manufacturers' data sheets).

The PV antibody (Sigma–Aldrich, Saint Louis, MO) recognizes a 12-kDa band on immunoblots of cultured nerve cells and tissue from human, monkey, rat, mouse, chicken, and fish (manufacturer's data sheet). There was no staining on control sections processed with omission of the primary antibody. Its staining pattern in cerebellar cortex was similar to two other descriptions of PV

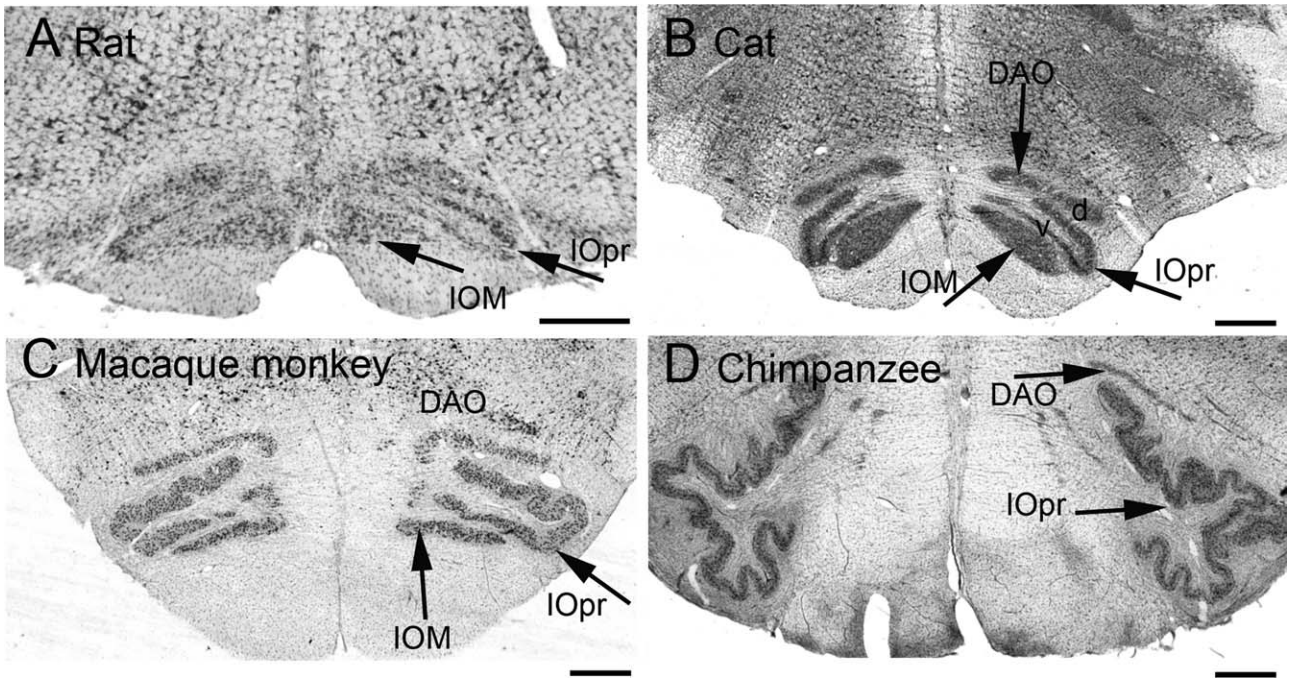

Fig. 1. CV-stained sections of the IOpr (arrows) in the rat (**A**), cat (**B**), macaque monkey (**C**), and chimpanzee (**D**) showing the different shapes. Scale bars = 1 mm. d, dorsal; DAO, dorsal accessory olive; IOpr, principal nucleus of the IO; IOM, medial nucleus of the IO; and v, ventral.

expression in the human cerebellum (Yu et al., 1996; Milosevic and Zecevic, 1998); neither of those studies used an antigen-retrieval (AR) protocol.

Immunohistochemistry

For single-label immunohistochemistry, we used procedures previously described for sections from these cases (Baizer et al., 2007b; Baizer and Broussard, 2010). Briefly, sections through the IOpr were first treated with an antigen retrieval protocol. Sections were removed from the formalin, rinsed in 0.1 M phosphate buffered saline (PBS; all rinses 3 × 10) and placed individually in glass jars in 20 cc of a sodium citrate–citric acid buffer. The sections were carefully unfolded in the jars. The pH of the buffer was 2.75 (for the SMI-32 Ab) or 8.0 (for the other Abs). A water bath was preheated to 85°C and the jars placed in it for 20–30 min. The jars were then removed from the water bath and cooled at RT for 20 min. The sections were removed from the jars and put into circular nets from Brain Research Laboratories (Newton, MA) and rinsed in PBS. They were then processed for immunohistochemistry as previously described. Immunoreactivity was visualized with a DAB protocol or the glucose oxidase modification of it (Adams, 1981; Gilligan et al., 2004; Van der Gucht et al., 2006).

Slides were examined with a Leitz Dialux 20 microscope, and digital images (1600 × 1200 pixels) of selected sections captured with a SPOT camera mounted on that microscope. We used Adobe Photoshop software to adjust brightness and contrast of images and to assemble the figures.

Lipofuscin

Neurons in the IO have long been known to accumulate lipofuscin with age (Mann and Yates, 1974; Mann et al., 1978). To assess the presence of lipofuscin in our cases, sections were rinsed, mounted on gelled slides, and coverslipped with Vector Hardset Mounting Medium. Slides were then examined with a Zeiss AxioImager fluorescence microscope. We compared filter sets for fluorescein isothiocyanate (FITC), Cy3, and Cy5 and found the brightest autofluorescence with the Cy3 filter set. Digital images were captured using Zeiss software, brightness and contrast adjusted with that software and then images exported and the figures assembled using Photoshop.

Quantification of IOpr Volume and Folding in Humans

We quantified the volume of the left and right IOpr from Nissl-stained serial sections in a total of nine human cases, including six from the Witelson Collection, and an additional three cases of archived slides from the Department of Psychiatry, University of Geneva School of Medicine, Geneva, Switzerland (Dr. C. Bouras) that had also been used in previous research (Sherwood et al., 2005). The Cavalieri method was used to estimate the volume of each nucleus (Gundersen et al., 1988) from digital flatbed scans (47.2 pixels/mm) using a 200-μm counting grid in ImageJ software, 1.37v. For each side, 10–16 sections were analyzed at intervals of 300, 600, or 1,000 μm between sections. Sampled sections from each specimen were chosen at equidistant intervals for each IOpr and the starting section was picked randomly from the first interval. The coefficient of error of the volume estimate (Gundersen et al., 1999, $m = 1$)

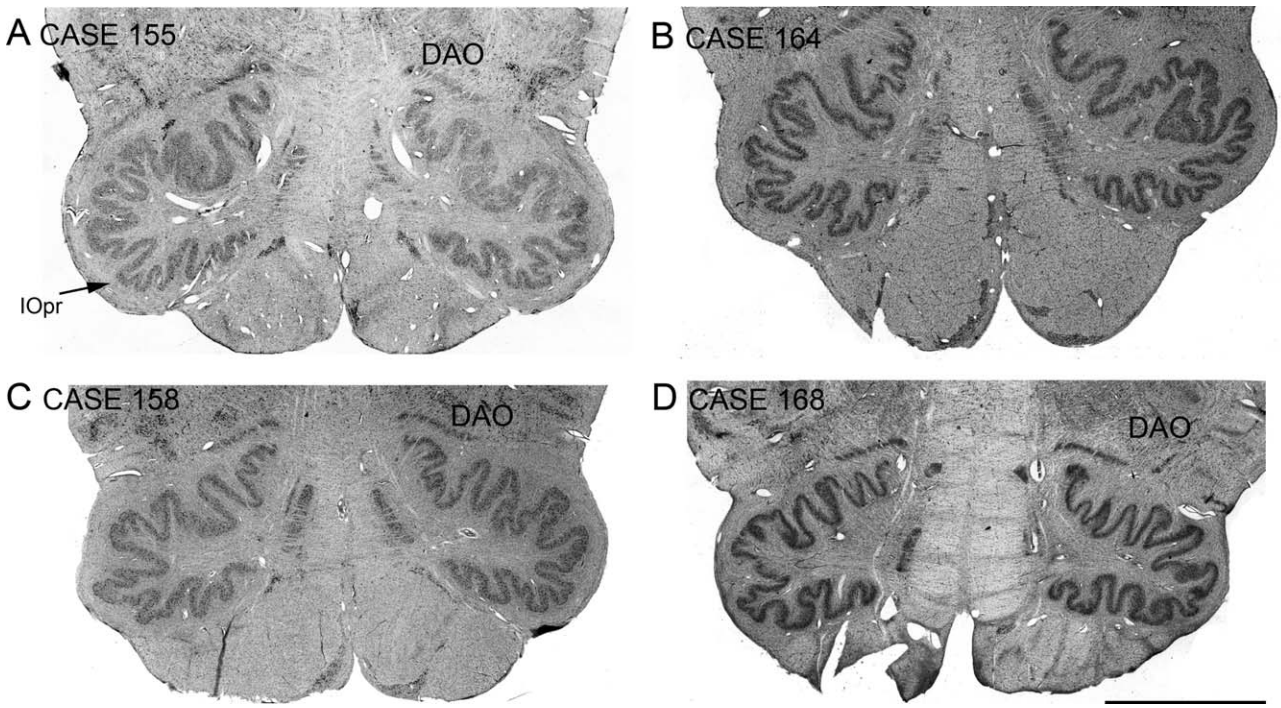

Fig. 2. CV-stained sections of the IO from Cases 155 (**A**), 164 (**B**), 158 (**C**), and 168 (**D**). For each case, the images are low magnification of sections through the IOpr at a level about 7 mm rostral to its caudal limit. Note the left–right asymmetry in folding patterns in each case. Scale bar = 5 mm.

was less than 0.05 for each specimen. In addition, a folding index was calculated for each IOpr. The folding index was measured in the same sections used for volume estimation by tracing a line contour around the lateral outer perimeter of the nucleus and another line following the complex folding of the IOpr lamina. The ratio of the folded IOpr lamina to its outer perimeter was calculated as the folding index. A higher folding index value indicates a greater complexity of folding.

RESULTS

Shape and Extent of the Principal Olive

Figures 1–3 show sections from rat, cat, rhesus monkey, chimpanzee, and human that illustrate the species differences in the size and shape of the IOpr. In the rat and cat, the IOpr consists of two lamellae, a dorsal and a ventral. In the chimpanzee, the IOpr is considerably enlarged and has the form of a flat ribbon with many infoldings. The IOpr is even more enlarged in the human. In humans, the IOpr is also a flat ribbon (about 200–300 μm across), with many infoldings. It extends over about 14 mm in the rostral–caudal direction (range, 12–16 mm; Table 3) and is surrounded by a fiber capsule called the "amiculum olivae" (Gautier and Blackwood, 1961). The human IOpr is sometimes described as consisting of three lamellae (i.e. a dorsal, ventral, and lateral; Lasn et al., 2001), but as shown in Figs. 2 and 3, there are no clear demarcations between dorsal and lateral or lateral and ventral lamellae. It has also been described as a "crumpled purse," with the opening of the purse called the hilus (Cunningham, 1903). Figures 2A–D and 3A–C show CV-stained sections from Witelson collection cases at a level about 7 mm rostral to the caudal limit of the IOpr. These images illustrate the differences in IOpr shape and folding pattern among these cases. There are individual differences in the relative heights and widths of the IOpr, and especially in the number and relative location of the deeper (primary) and shallower (secondary) sulci. Although the overall width and height of the IOpr are similar on both sides of a single case, the folding pattern differs between sides, again especially marked in the numbers and depths of secondary sulci in individual cases (compare left and right sides, Figs. 2 and 3).

Three-Dimensional Model of the IOpr

To visualize the 3D complexity of this structure, we constructed a model of the IOpr based on parasagittal sections (using the case from the Barrow Neurological Institute). Figure 4 shows four images of this model from different perspectives (a 3D rotating movie is included as Supporting Information). The hilus of the IOpr is directed ventro-medially and the larger dorsal lamella shows a number of sulci. Four deeper sulci are depicted in Fig. 4, dorsal view. In addition, the IOpr has numerous folds and indentations. The volume we obtained from this IOpr reconstruction is 85 mm^3 and the surface area is 547 mm^2 (including the outer and inner surface). The thickness of the IOpr lamella is 0.31 mm.

Asymmetry

The asymmetry in folding pattern was consistent over the rostrocaudal extent of the IOpr. Figure 5 shows the

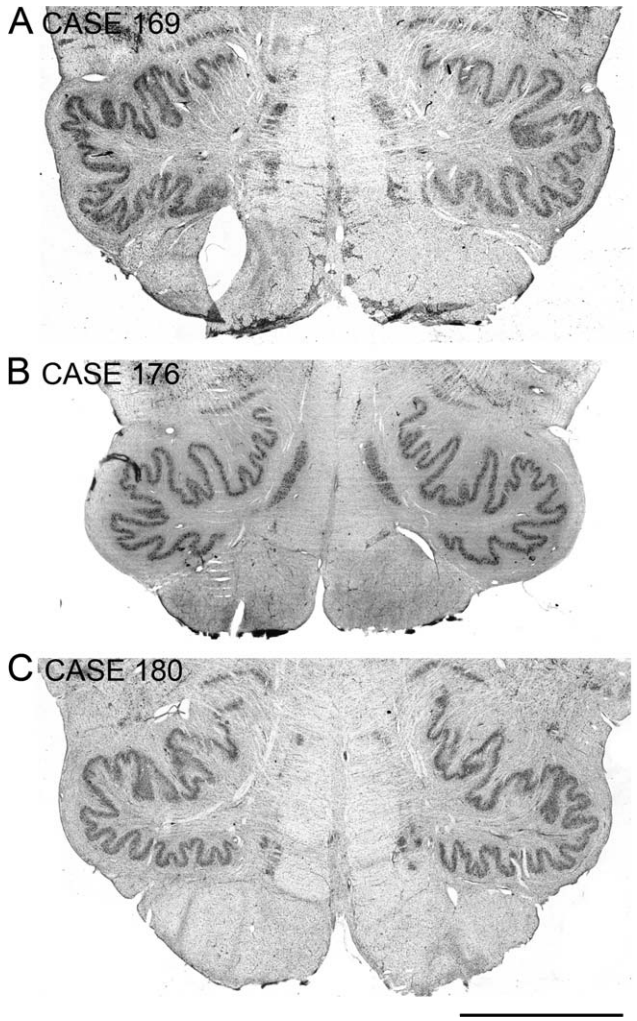

Fig. 3. CV-stained sections from Cases 169 (**A**), 176 (**B**), and 180 (**C**). All sections are at a level 7 mm rostral to the caudal limit of the IOpr. Scale bar = 5 mm.

IOpr on sections about 2 mm apart from a single case; the left–right asymmetry is present at all levels. At some levels (Fig. 5B–E), a deeper sulcus is seen that can also be seen on our 3D model (Fig. 4).

To assess whether this asymmetry was indicative of a quantitative difference between left and right sides, we calculated two measures of the IOpr, the volume and an index of folding (Table 3). The volume of the IOpr of humans (N = 9) was similar in the left (mean = 106.4 mm^3, SD = 14.2) and the right (mean = 104.9 mm^3, SD = 15.9). A paired samples t test did not reveal a significant difference in IOpr volume between sides ($t_8 = 1.01$, $P = 0.34$). Additionally, the folding index in the left (mean = 2.2, SD = 0.2) and right (mean = 2.2, SD = 0.2) also did not display any significant asymmetry (paired samples t test, $t_8 = 0.06$, $P = 0.96$).

Calretinin

Single-label immunohistochemistry experiments showed populations of neurons and fibers immunoreactive to CR.

TABLE 3. IOpr volumes (V, mm^3), folding index (FI) and rostrocaudal extent (mm)

Case	V-left	V-right	FI-left	FI-right	Extent (mm)
Human 164	91.8	79.6	2.10	2.13	12
Human 155	108.6	109.2	1.88	1.98	14
Human 158	128.4	129.9	2.31	2.28	16
Human 168	80.9	83.9	2.33	2.49	14
Human 176	106.8	103.8	2.43	2.34	15
Human 169	106.8	105.9	2.30	2.15	16
Human A33–02	118.6	119.5	2.17	2.16	20
Human G60–01	115.2	112.8	2.11	2.07	16
Human G98–99	100.8	99.8	2.10	2.13	16

However, the density and staining intensity of labeled neurons differed markedly among cases. Figure 6A shows a section from Case 176 and Fig. 6B a section from Case 168; there are many very darkly labeled neurons (examples at arrows) in each. In addition, there are labeled fibers running into the infoldings, roughly down the center (Fig. 6A, arrowhead). Figure 6C shows a very different staining pattern in Case 164. Although there are stained fibers seen in the infoldings, there are almost no labeled somata. Instead the cell bodies appear as white "ghosts" (Fig. 6C, example at arrow). In Case 155, there is good staining of fibers running perpendicular to the infolding (Fig. 6D, white arrowhead) and staining of a fascicle of fibers, showing that CR antigenicity is detected in this section. However, most somatas in the IOpr appear as white, unstained profiles (Fig. 6D, arrow). There was no obvious pattern to the distribution of stained and unstained somatas for these cases.

A different pattern is seen in Case 158. Figure 7A–C illustrates darkly labeled patches of CR-immunoreactive neurons (between arrowheads) in three closely spaced sections in Case 158. These patches of darkly labeled neurons are adjacent to stained neurons that were only very lightly labeled. Figure 7D shows an adjacent CV-stained section. The "patch" of darkly labeled neurons that is readily apparent with CR (A–C) is not visible in this stain (location indicated by arrow), suggesting a selective decrease of expression of CR in neurons outside the patch without major degenerative changes.

Calbindin

We also found populations of CB-immunoreactive neurons in the IOpr, and again there is variability among cases in the number of labeled neurons. In Cases 176 (Fig. 8A) and 168 (Fig. 8B), there are many CB-immunolabeled neurons (example in Fig. 8B, arrow). Figure 8A, white arrowhead shows a darkly labeled fiber fascicle that runs down the center of the infolding. By contrast, in Case 164 (Fig. 8C), there are almost no neurons in the IOpr that are stained for CB, and somata appear as white unstained profiles. This absence of staining for CB in the neurons of the IOpr does not reflect a general absence of the expression of CB in this case, as Purkinje cells and their axons in cerebellar cortex are darkly labeled (Fig. 8D).

Many neurons are labeled for CR and CB, suggesting that these two proteins may be colocalized. We were unable to assess double label using fluorescent secondary antibodies as we find considerable autofluorescence in the somata of neurons in the IOpr in the human cases

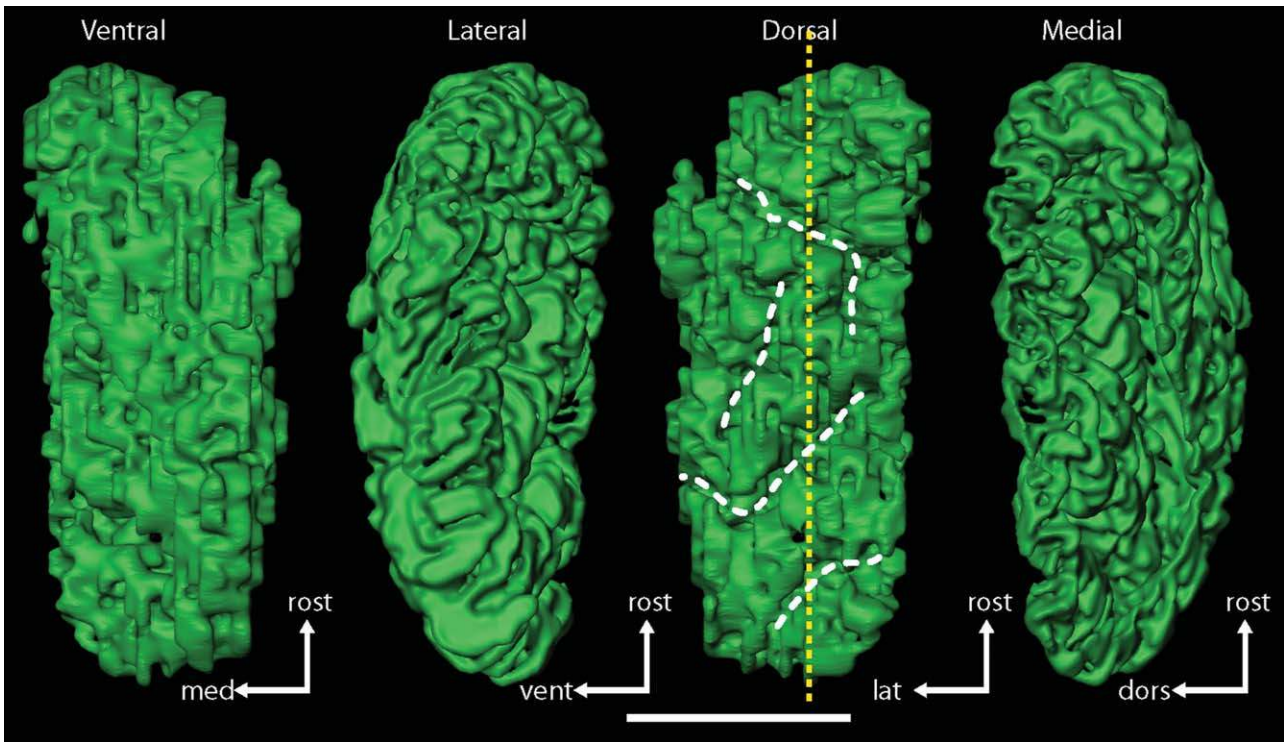

Fig. 4. Four views of a 3D model of the human IOpr constructed from parasagittal sections. The white stippled line marks four deeper sulci on the dorsal surface. The yellow stippled line marks position of the typical histological section shown in Supporting Information Fig. 1. Scale bar = 5 mm.

with good label for CR and CB (Fig. 15), a finding suggestive of the presence of lipofuscin in these neurons (Schnell et al., 1999).

Parvalbumin

With the third calcium-binding protein (PV), there are labeled fibers surrounding the IOpr (Fig. 9B, arrowhead) and running both parallel and perpendicular to the folia (Fig. 9A,B). There are no labeled neurons in the IOpr, and labeling of processes in all cases is similar.

nNOS and NPNFP

We also examined the expression of other markers that have been helpful in our analysis of the human vestibular brainstem (Baizer and Broussard, 2010; Baizer et al., 2011). For nNOS, in all cases, the IOpr ribbon is densely stained (Fig. 10A–C shows three examples). At higher magnification, this label is seen to be punctate, presumably consisting of nitrergic terminals of axons ending in the IOpr (Fig. 10B). Usually, cell bodies are not stained, but appear as white "ghosts." In some cases, however, there are scattered nNOS immunoreactive somata (e.g. Cases 168, Fig. 10B, and 176, Fig. 10D, arrows); no staining of somata is seen in Case 164 (A). The absence of stained neurons in the IOpr again does not reflect an absence of nNOS staining in this case; the arrows show darkly labeled cell groups outside the IOpr. The density of labeled neurons was never as great as with CB or CR.

Individual variability in staining of somata is also seen with an antibody to NPNFP. There were stained fibers running down the center of the infoldings (Fig. 11A, top arrowhead) as well as staining of the "amiculum olivae" (Fig. 11A, bottom arrowhead). There were also scattered stained somata in several cases (Fig. 11A–C) but in these cases the number of stained neurons is not as high as with CR or CB.

GAD

We used an antibody to glutamic acid decarboxylase (GAD) to assess the presence of inhibitory neurons (releasing the transmitter gamma-aminobutyric acid, GABA) in the IOpr. Figure 12 illustrates the dense "ribbon" of staining following the contours of the IOpr (A, Case 155; B, Case 158; and C, Case 176). At higher magnification, this staining appears punctate, often surrounding somata (Fig. 12D, arrow) and probably corresponds to the terminals of gamma-aminobutyric acid (GABA) in the IOpr. Very few labeled somata are seen in these sections; instead, there are unstained profiles (example at Fig. 12B, arrow), presumably the large, unstained projection neurons. The staining pattern is similar in all cases.

CR: Other Species

Because the expression of CR in the IOpr had not been previously reported in rodents (Arai et al., 1991; Résibois and Rogers, 1992), we asked whether the expression of CR is unique to the human. We examined archival stained sections and found neurons stained for CB and CR in the IO of cat, rhesus monkey, and chimpanzee.

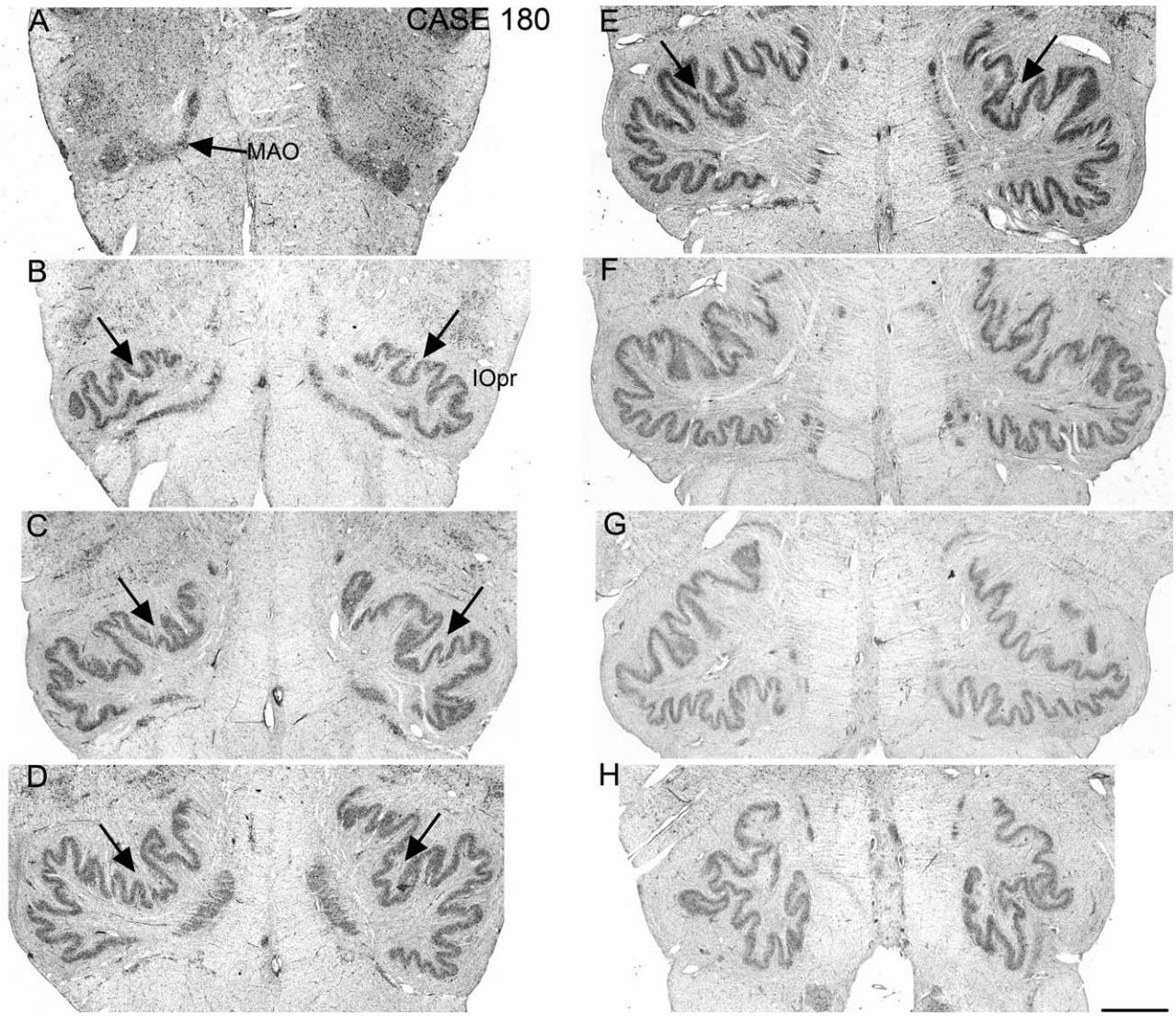

Fig. 5. CV-stained sections about 2 mm apart through the rostrocaudal extent of the IOpr in Case 180. **A**: The most caudal. **B–E**: The arrows indicate a major sulcus that is seen bilaterally. Note the different folding patterns on the left and right sides at all rostrocaudal levels. Scale bar = 1 mm.

We also wondered if individual variability in the numbers of IOpr neurons labeled for CR, CB, NPNFP, and nNOS might be unique to humans, as our data in other species had not shown similar variability. We, therefore, looked at great apes, the closest living relatives of humans using archival CV-stained sections from a total of six chimpanzees (five archived cases as well as the one sectioned for this study), four gorillas, and four orangutans. The IOpr in the great apes is not as complexly folded as in the human (compare Fig. 1D with Figs. 2 and 3), and the IOpr ribbon is thinner. Figure 13 shows images of the IOpr on CV-stained sections from six chimpanzees. The arrangement of neurons in the chimpanzee IOpr is different from that in the human. For five of the six cases, along the inner and outer edges of the IOpr perimeter, there are sets of closely spaced neurons oriented with their long axes perpendicular to the IOpr ribbon (arrows in Fig. 13A–E). For the sixth case (Fig. 13F), this arrangement is not seen, and there are fewer stained neurons overall. This outlining of the perimeter of the IOpr is not seen in the human sections in which neurons appear randomly scattered throughout its width (e.g. Figs. 6A,B and 7D). This clustering of neurons along the outline of the IOpr was observed in two out of the four orangutans and in none of the gorillas. We also assessed the labeling patterns for several markers in a chimpanzee. Figure 14 shows the IOpr in a chimpanzee (Case AN, female, age 45) with somata labeled for CR (Fig. 14A), CB (Fig. 14C), nNOS (Fig. 14B), and NPNFP (Fig. 14D). There were no patches of labeled neurons or white somata ghosts in any of the sections regardless of antigen. Also compared with the human, many more labeled somata were seen outside the IOpr ribbon.

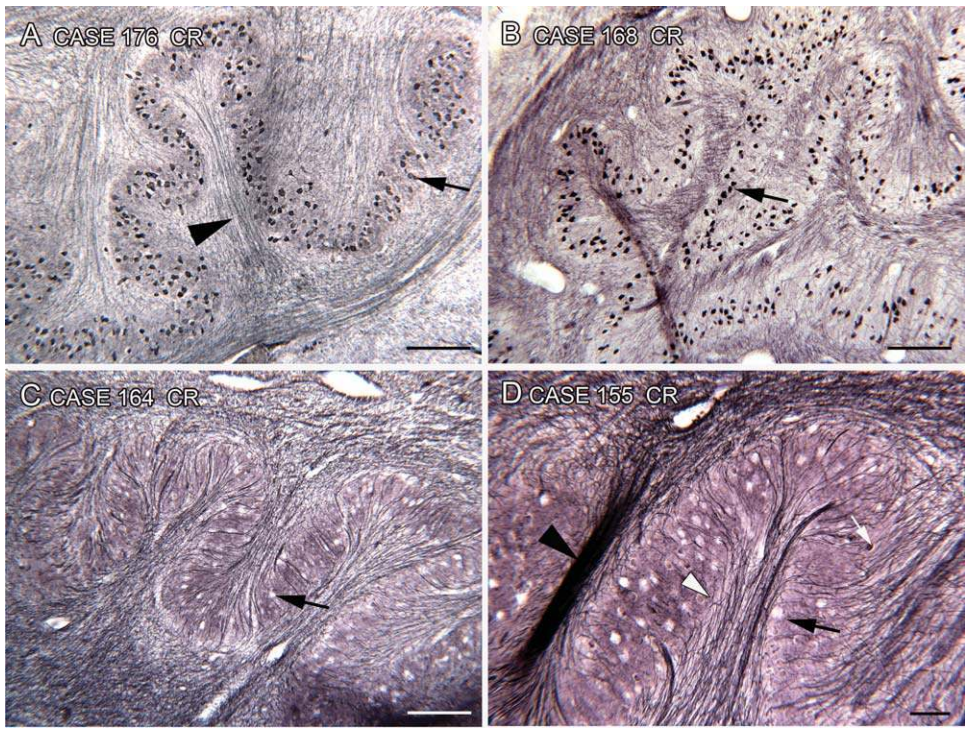

Fig. 6. Expression of CR in the IOpr of four cases. **A**: Case 176. There are many neurons labeled for CR (arrow) and stained fibers running the length of the infolding (arrowhead). **B**: Case 168. This case also has many stained neurons; example at arrow. Scale bars = 250 μm. **C**: Case 164. This case has much sparser and lighter label; note the white "ghosts" of somatas, example at arrow. Scale bar = 250 μm. **D**: Case 155 has label of fibers (white arrowhead) but not of somatas (black arrow). There is also a darkly labeled thick fascicle of fibers, black arrowhead. Scale bar = 100 μm.

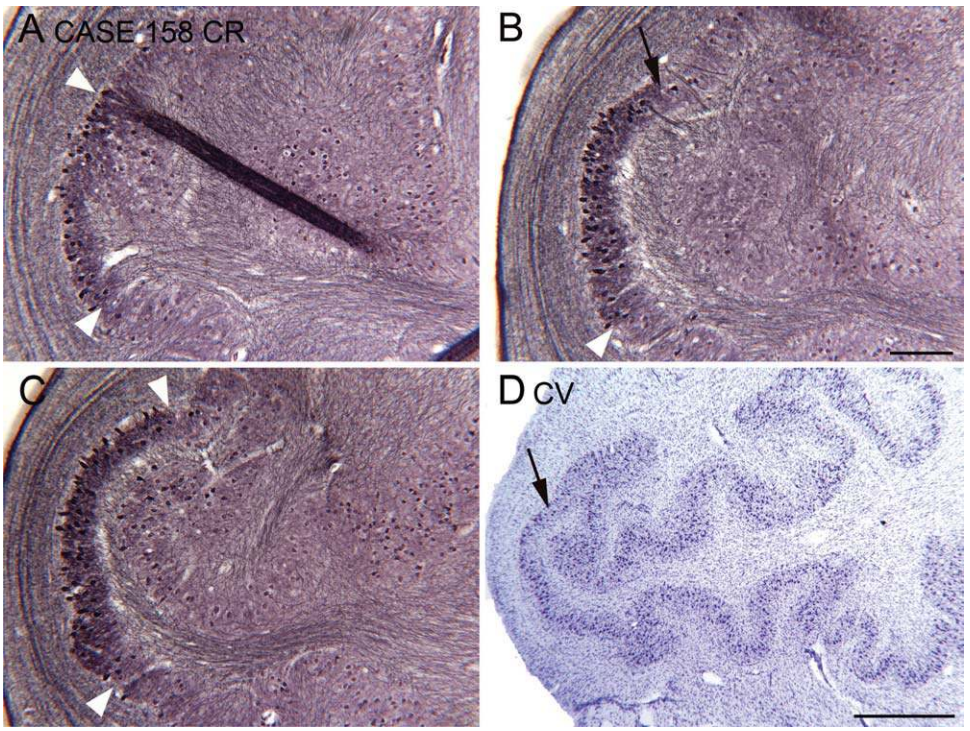

Fig. 7. **A–C**: Three sections from Case 158 about 200 μm apart showing a darkly labeled patch of CR-immunoreactive neurons at the lateral edge of the IOpr (white arrowheads). Scale bar = 250 μm. **D**: CV-stained section adjacent to the section in B; the black arrow is an alignment point for B and D. Scale bar = 1 mm.

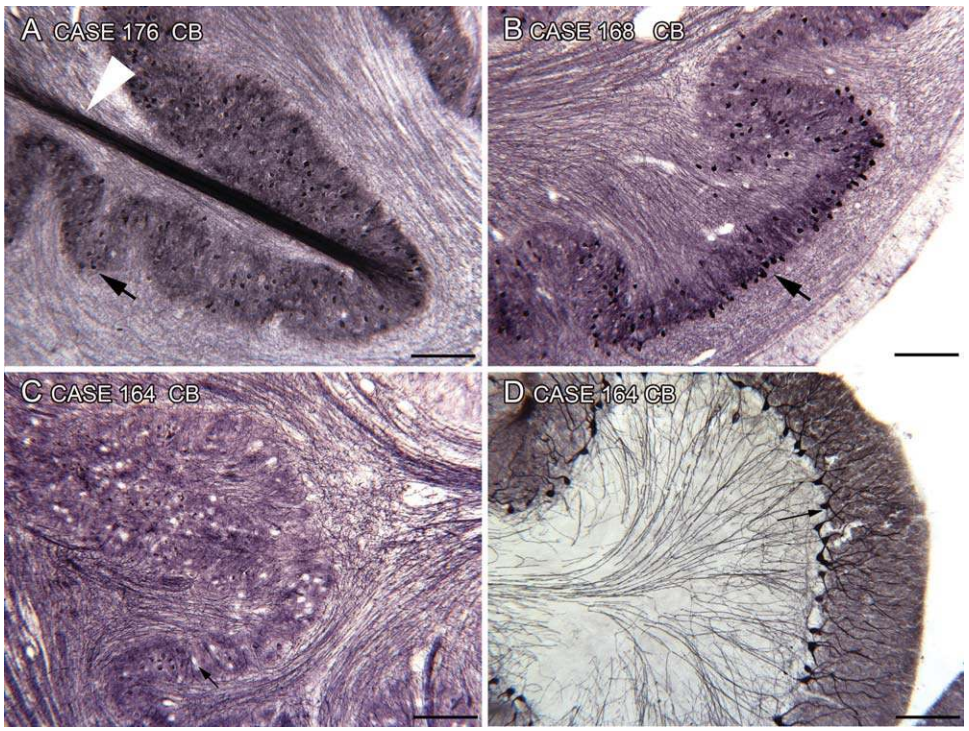

Fig. 8. CB in the IOpr. **A**: Case 176. **B**: Case 168. Both cases have many darkly labeled somatas in the IOpr (small arrows). The arrowhead in A marks a darkly labeled fascicle of fibers. Scale bars = 250 μm. **C**: Case 164. There are few labeled neurons in this case; the arrow shows the profile of an unstained soma. Scale bar = 250 μm. **D**: Dark CB labeling in Purkinje cells of cerebellar cortex of Case 164. Scale bar = 250 μm.

Lipofuscin in the IOpr

We also wondered if the neurochemical differences among species might be related to known species differences in the accumulation of lipofuscin, the "age pigment," in neurons of the IOpr (Dayan, 1971; Mann and Yates, 1974; Mann et al., 1978). Figure 15 shows images of autofluorescence in the IOpr of four human cases, one monkey, and one chimpanzee. The cases vary in the apparent brightness and density of autofluorescent neurons, but they are present in all of them. There are also fluorescent neurons in the macaque monkey (age unknown) and the chimpanzee (age 45); however, these species did not show the variability in staining with the markers we used.

DISCUSSION

We have studied the extent, configuration, and neurochemical properties of the IOpr in the human. Our results show individual variability in the IOpr folding pattern, overall extent, and in the neurochemical properties of neurons. We will consider these results in the context of the structures with which the IOpr is directly and indirectly connected, the cerebellum and the cerebral cortex.

Enlargement and Asymmetry of the Human IOpr

The IOpr enlargement is seen as an elongation and narrowing of the lamellae with the development of many infoldings. This is in contrast to the enlargement of other IO components seen in other species. For example, the entire medial olive is greatly enlarged in the porpoise (Kooy, 1917); there is no transformation of the structure to a folded sheet. The enlargement of the human IOpr is reminiscent of the expansion of both cerebral and cerebellar cortex, both of which remain sheets with the development of sulci and gyri and a complex folding pattern. The increase in folding in the IOpr is similar to what is seen in the human dentate nucleus (Sultan et al., 2010). Cerebral and cerebellar cortex, the IOpr, and the dentate nucleus all show complex folding patterns in human; could the same factors affect development in all? It has been argued that the enlargement of the cerebral cortex as a folded sheet is determined by the cortical column as the fundamental unit of processing (Rakic, 1995). Columnar processing of information has not been proposed for either the dentate nucleus or the IOpr, suggesting that there is some other critical organizing factor for these structures.

The individual variability in folding pattern and left–right asymmetry in the IOpr is easily seen when bilateral sections from multiple cases are compared. It has not been remarked on previously; most reports show only one side of the brainstem (Kooy, 1917; Olszewski and Baxter, 1982; Paxinos and Huang, 1995) and are based on a limited number of cases. What is the significance of the asymmetry? In cerebral cortex, asymmetry between the hemispheres reflects quantitative differences in size and structure related to both language and handedness. For example, the size of the planum

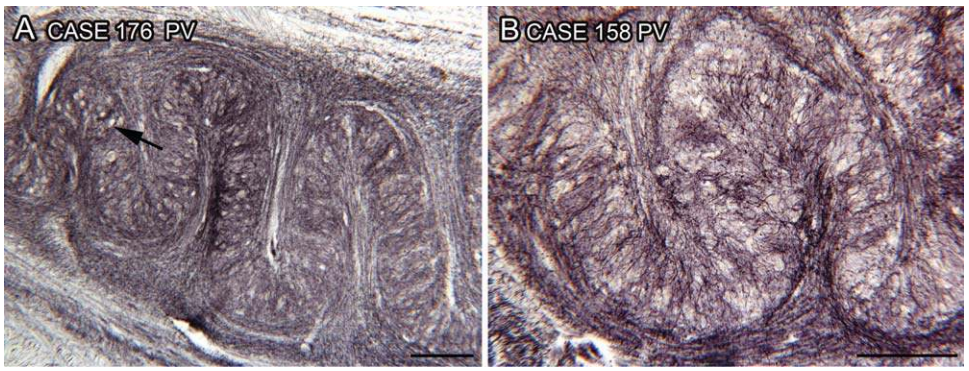

Fig. 9. PV immunoreactivity in the IOpr in Cases 176 (**A**) and 158 (**B**). Note the labeled fibers and the absence of labeled neurons in both cases. Arrow marks an unstained soma. Scale bars = 250 μm.

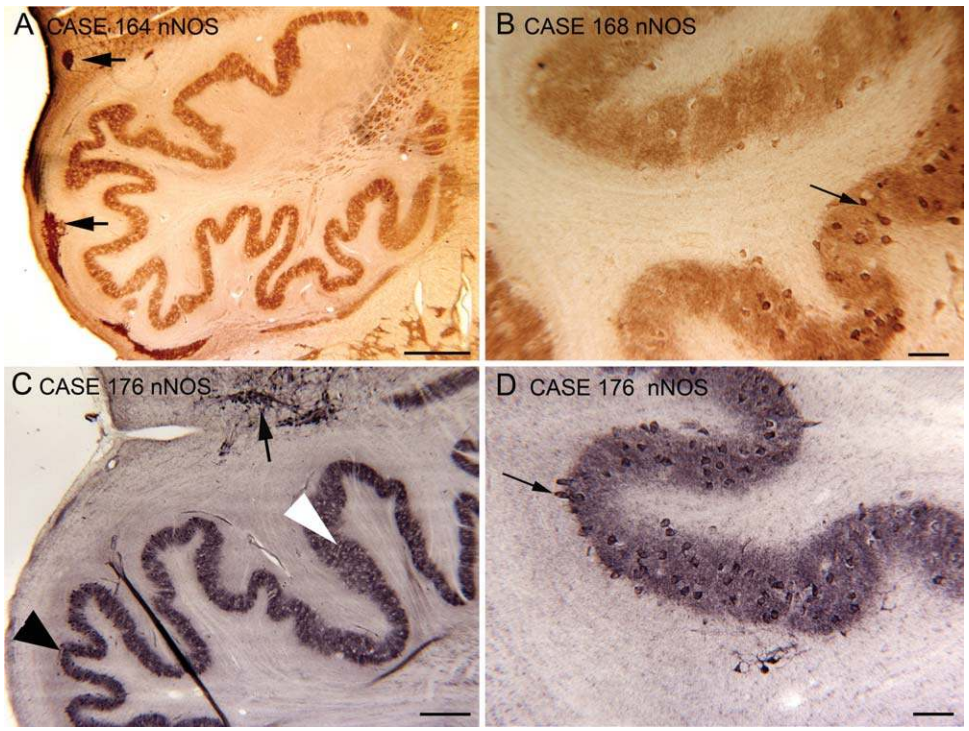

Fig. 10. Immunoreactivity to nNOS in the IOpr. **A**: Case 164, DAB visualization. The entire IOpr is outlined by punctate label. The arrows indicate darkly stained neurons outside the IOpr. **B**: Case 168, DAB visualization. In this case, there are stained somatas (arrow) and many that are not stained. **C** and **D**: Case 176, Glucose Oxidase visualization. In this case, the IOpr ribbon is darkly stained; the lower magnification image shows regions of stained somatas (black arrowhead) and regions where only the white "ghosts" of neurons are seen (white arrowhead). The black arrow indicates a region of stained neurons dorsal to the IOpr. D: Region of the IOpr in Case 176 with stained somatas (example at arrow) some of which are on the edges of the stained ribbon. Scale bars = 250 μm.

temporale is greater on the side mediating language (Geschwind and Levitsky, 1968; Wada et al., 1975; Galaburda et al., 1978); for motor areas, more subtle differences related to handedness have been reported, for example, in the depth of the central sulcus (Amunts et al., 1996). Because the IOpr participates in the corticocerebellar circuits implicated in control of the hand and fingers (Glickstein et al., 2005), and possibly also circuits for language and cognitive function, we quantified left–right differences. We compared two relatively simple measures of complexity for the IOpr, volume and folding complexity, and found no systematic left–right differences. One earlier study did report asymmetry, with the IOpr on the left beginning and ending 1 mm caudally to the IOpr on the right (eight cases; Moatamed, 1966). However, we did not see a consistent difference among our cases in the caudal appearance of the IOpr.

Comparison of Neurochemical Properties with Other Species

We found expression of five markers, CR, CB, nNOS, and NPNFP in at least some IOpr neurons, and

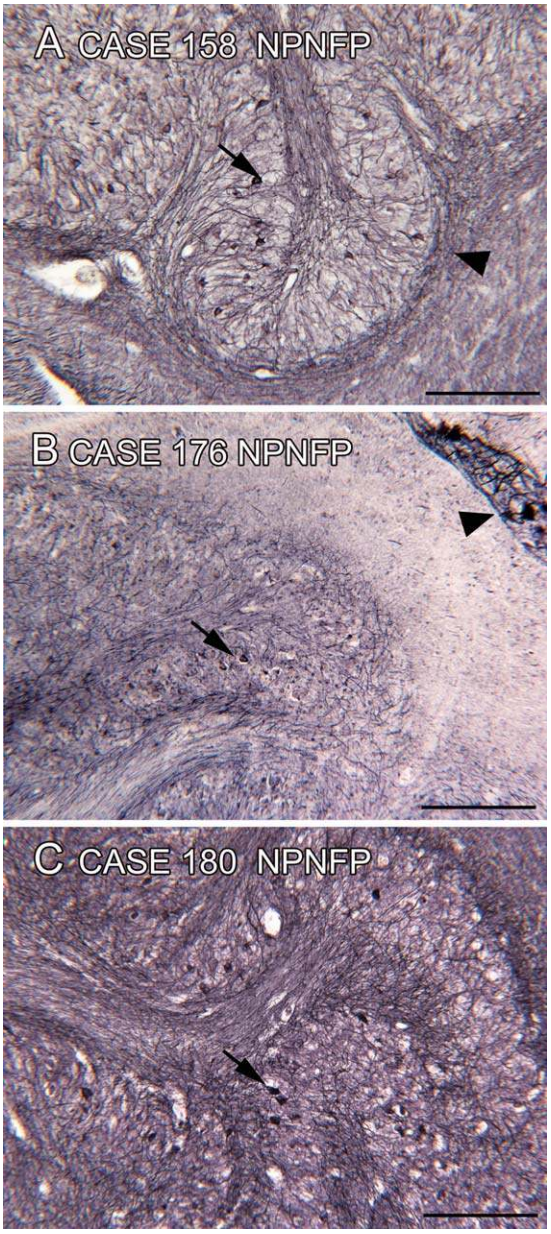

Fig. 11. Scattered neurons in the IOpr of Cases 158 (**A**), 176 (**B**), and 180 (**C**) showing NPNFP immunoreactivity. The arrows indicate scattered labeled neurons. The arrowheads in A show labeled fibers surrounding the IOpr and running down the center of the infolding. Scale bars = 250 μm.

expression of PV, CB, CR, nNOS, and NPNFP consistently in fibers. How do these results compare with other species?

We show CR immunoreactivity in neurons of the IOpr in the human and chimpanzee; it is a common feature of all species we have studied (cat, squirrel monkey, and rhesus monkey, unpublished observations). Earlier studies in rodents did not report CR label in IO neurons (Arai et al., 1991; Résibois and Rogers, 1992; Paxinos et al., 1999); this is probably to reflect a difference in methods rather than a true phylogenetic difference. Expression of CB in IO has been reported for rats and humans; we also saw CB in the IO of cats and macaque monkeys (Celio, 1990; Rogers and Résibois, 1992; Wassef et al., 1992; Paxinos et al., 1999; Nag and Wadhwa, 2004). The absence of PV immunoreactivity in neurons of the IO in any species is also consistent with previous results from rats (Celio, 1990; Wassef et al., 1992; Paxinos et al., 1999).

The finding of nNOS label in the neuropil and some neurons of the IOpr is not in agreement with studies of rodents using immunohistochemistry (Rodrigo et al., 1994) or histochemistry for Nicotinamide adenine dinucleotide phosphate (NADPH)-diaphorase (Paxinos et al., 1999). We have also seen neurons immunoreactive for nNOS in the IO of cats and macaque monkeys (unpublished observations) and in the chimpanzee, suggesting that at least some IOpr neurons normally express nNOS. However, NADPH or nNOS may be increased in the IOpr following injury to the axons of IO neurons (Buffo et al., 1998, 2003; Carulli et al., 2004); we cannot rule out the possibility that the label in all species might reflect some reactive process affecting only subsets of neurons.

We saw NPNFP expression in some neurons of the IOpr in humans and in all neurons of the chimpanzee. We have also seen immunolabel for NPNFP in neurons of the cat and monkey IO (unpublished observations). In rodent, NPNFP label was not shown in the IO (Paxinos et al., 1999).

Possible Sources of PV, CR, nNOS, and NPNFP Fibers

The fibers labeled by proteins that were also observed in IOpr somata (CR, CB, and NPNFP) may be olivocerebellar efferents. The large fascicles of labeled fibers are probably to be groups of axons that cross the midline to travel to the cerebellum in the contralateral inferior cerebellar peduncle. CB in olivocerebellar fibers in human has been reported (Nag and Wadhwa, 2004). However, some labeled axons may be afferents to the IO. CR-immunolabeled afferent fibers may include the GABAergic afferents from the deep cerebellar nuclei or spino-olivary axons (Arai et al., 1991). There are neurons in the human cerebellar dentate nucleus that express CR (Baizer, unpublished observations) and a GABAergic projection from deep cerebellar nuclei to the IO has been shown in other species (Martin et al., 1976; Best and Regehr, 2009). Cortico-olivary fibers may be labeled with NPNFP as cortical pyramidal neurons express this protein (Hof and Morrison, 1995; Hof et al., 1996, 1997). There are brainstem oculomotor neurons that express PV (Horn et al., 1995; Horn and Büttner-Ennever, 1998); nNOS is expressed in the nucleus prepositus, PrH (Moreno-López et al., 2001); both regions may be sources of afferents to the IO. The IO also gets input from spino-olivary fibers (Brodal et al., 1950) and populations of axons immunoreactive for CB, CR, and PV have been reported in rat spinal cord (Celio, 1990).

Unique Neurochemical Properties of the IO

The density of labeled neurons in the IOpr with CR and CB in human cases 168 and 176, in the macaque monkey, and the chimpanzee suggests that these proteins may be colocalized. (The autofluorescence in all

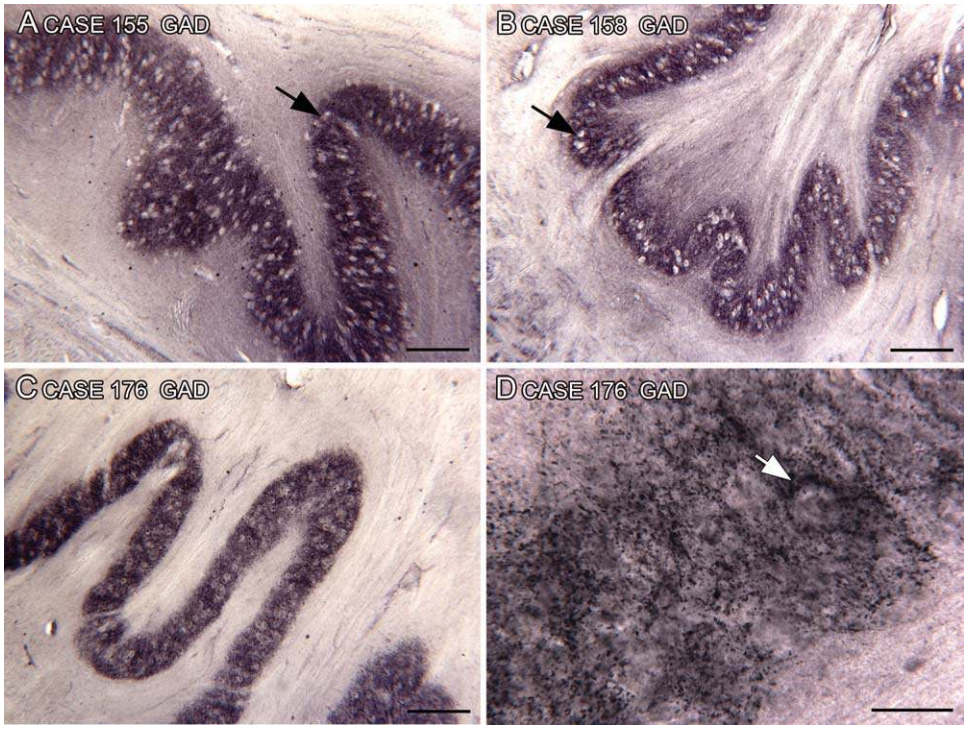

Fig. 12. Expression of GAD65/67 in the IOpr. **A–C**: Photomicrographs showing dense label of the IOpr ribbon with unstained white somata (arrows) in three different cases. Scale bars = 250 μm. **D**: The label consists of puncta probably labeled terminals of GABAergic afferents; the arrow indicates an unstained soma surrounded by labeled puncta. Scale bar = 100 μm.

these cases precluded using fluorescent secondary antibodies to assess colocalization directly.) In the cerebral cortex, these proteins are typically found in different populations of GABAergic interneurons (DeFelipe, 1999, 2002; Hof et al., 1999; Paxinos and Franklin, 2001) and not in excitatory projection neurons. In the cerebellar cortex, CB and PV are found in Purkinje cells (Celio, 1990 for rat and unpublished observations in human cerebellar cortex), whereas CR immunoreactivity is found in unipolar brush cells and Lugaro cells (Floris et al., 1994; Nunzi et al., 2002). In cerebral cortex, NPNFP is seen in projection neurons and is not typically colocalized with calcium-binding proteins (Van Brederode et al., 1990; Glezer et al., 1993; Hof and Morrison, 1995; Hof et al., 1996, 1997). One exception is a population of CB-immunoreactive pyramidal neurons in cortical layers II and III (Hof and Morrison, 1991; Hayes and Lewis, 1992; Kondo et al., 1999) and another is CR-immunoreactive pyramidal neurons in human and great ape anterior cingulate cortex (Hof et al., 2001).

Reliability of the Neurochemical Characteristics of the Human IOpr: Lipofuscin and RNA

Our cases showed considerable individual variability in the numbers of neurons labeled with different markers. This variability is seen for the proteins that are expressed in somata (CR, CB, nNOS, and NPNFP) but not for those that are expressed only in processes (PV and GAD). Does this variability truly reflect the neurochemical composition of the neurons of the IOpr in different cases or could these differences simply reflect methodological artifact relating to variation in Post Mortem Intervals (PMIs) and time in formalin? There are several reasons why we do not think that the individual differences are due to differences in tissue history. First, the PMIs for all the cases from the Witelson collection are very short and similar among cases (Table 1). The times in formalin are relatively long, but, again, similar among cases (Table 1). If the variability reflects overall loss of the protein from the tissue, one would expect loss of label in processes as well as somata. However, in the cases with fewer neurons in the IOpr stained for CR and CB (Cases 155, Fig. 6D; 164, Fig. 6C and 169; Case 158, Fig. 7, had "patches" of CR-stained neurons), fibers in the IOpr are well-stained for these proteins (see CR fibers in Figs. 6D for Case 155, and 6C for Case 164 and Fig. 8C for CB fibers in Case 164). Further, in those same cases, there is good and consistent staining for the same markers in other brainstem structures. This is illustrated for nNOS expression in the brainstem for Case 164 in Fig. 12A (arrows indicate nNOS staining outside the IOpr). Figure 8D shows consistent staining for CB in Purkinje cells of the cerebellar cortex for Case 164.

We have also found consistent immunostaining in these cases using the same antibodies in other brainstem structures (Baizer et al., 2007b; Baizer and Broussard, 2010). Table 4 lists the cases shown in this report and the figure numbers in the two earlier reports in which we illustrated staining for these markers in other

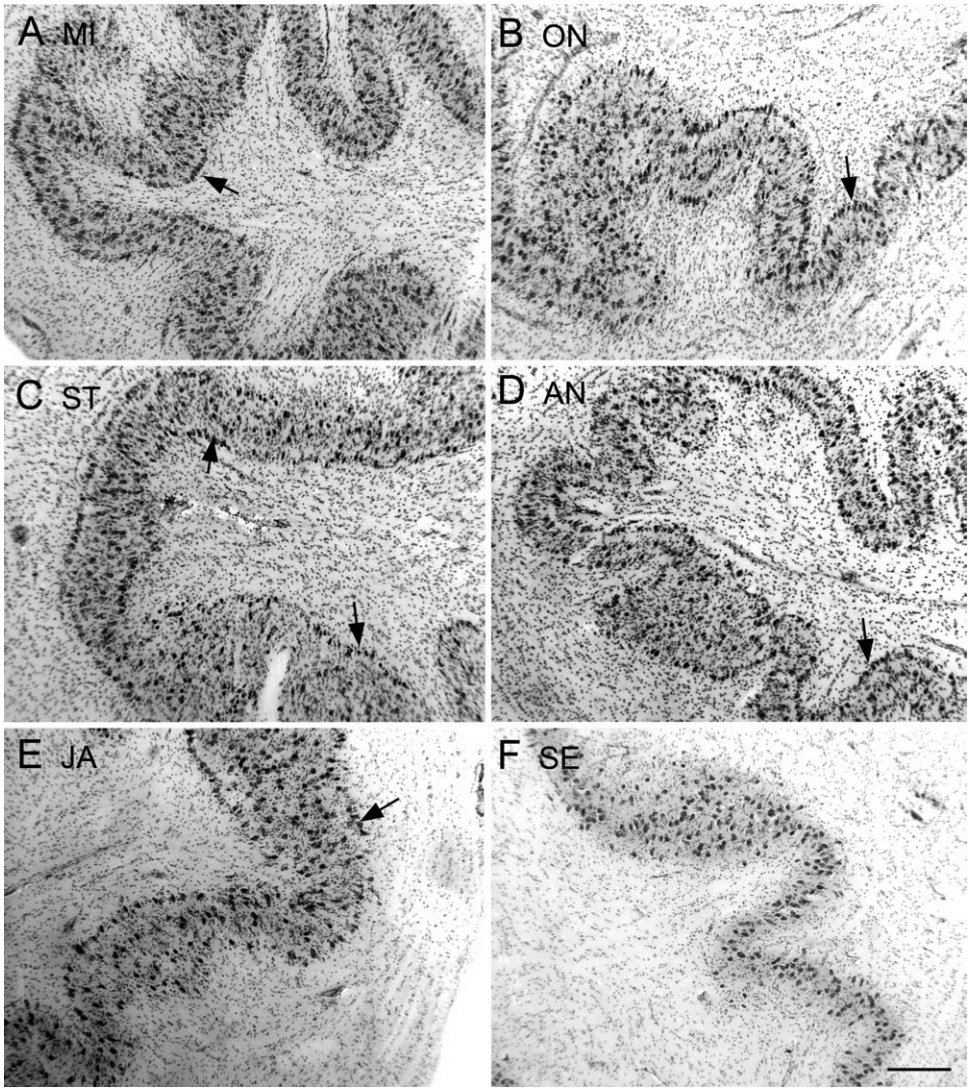

Fig. 13. CV-stained sections through the IOpr of six different chimpanzees (MI, ON, ST, AN, JA, and SE). The arrows indicate closely spaced labeled neurons at the inner or outer edges of the IOpr ribbon. Scale bar = 250 μm.

structures. For example, in Case 164 with CR, CB, and nNOS, there are very few stained somata in the IOpr (Figs. 6C, 8C, and 10A). However, we previously showed good CR staining in cells of the medial vestibular nucleus (MVe, Figs. 2A–E and 4B, Baizer and Broussard, 2010), and staining for nNOS in neurons of the external cuneate nucleus (ECu, Fig. 12, Baizer and Broussard, 2010) of this case. We, therefore, argue that the differences in staining of somata in the IOpr for CB, CR, nNOS, and NPNFP among cases or different regions of the IOpr for same case (e.g. Case 158, CR) described here reflect real biological variation.

This interpretation is strongly supported by the data on lipofuscin accumulation in the IOpr. Lipofuscin is the "aging pigment" that builds up in postmitotic neurons with age (Brizzee, 1981; Terman and Brunk, 2004; Gray and Woulfe, 2005). Many studies have shown that lipofuscin accumulation is especially pronounced in neurons of the IO, and most find that there is a linear accumulation of lipofuscin with increasing age, albeit with a lot of variability (Issidorides and Shanklin, 1961; Barden, 1970; Brizzee et al., 1974; Mann and Yates, 1974; Mann et al., 1978; Drach et al., 1994). One study measured levels of lipofuscin among neurons in the IO of single individuals and found a high degree of cell to cell variability (Drach et al., 1994). Other neuronal changes accompany, and may even be caused by, this pigment accumulation (Terman and Brunk, 2004; Gray and Woulfe, 2005); these changes include a decrease in nucleolar volume and size of the somata (Mann et al., 1978; Pesce et al., 1990). Most interestingly, for the present results, there is also a decrease in ribosomal RNA, the consequence of which would be decreased or altered protein synthesis (Mann and Yates, 1974; Mann et al., 1978). The neurochemical variability that we see, then, most probably reflects the alterations in protein synthesis that accompany pigment accumulation and RNA loss in the human. Our data suggest that this happens at different rates for

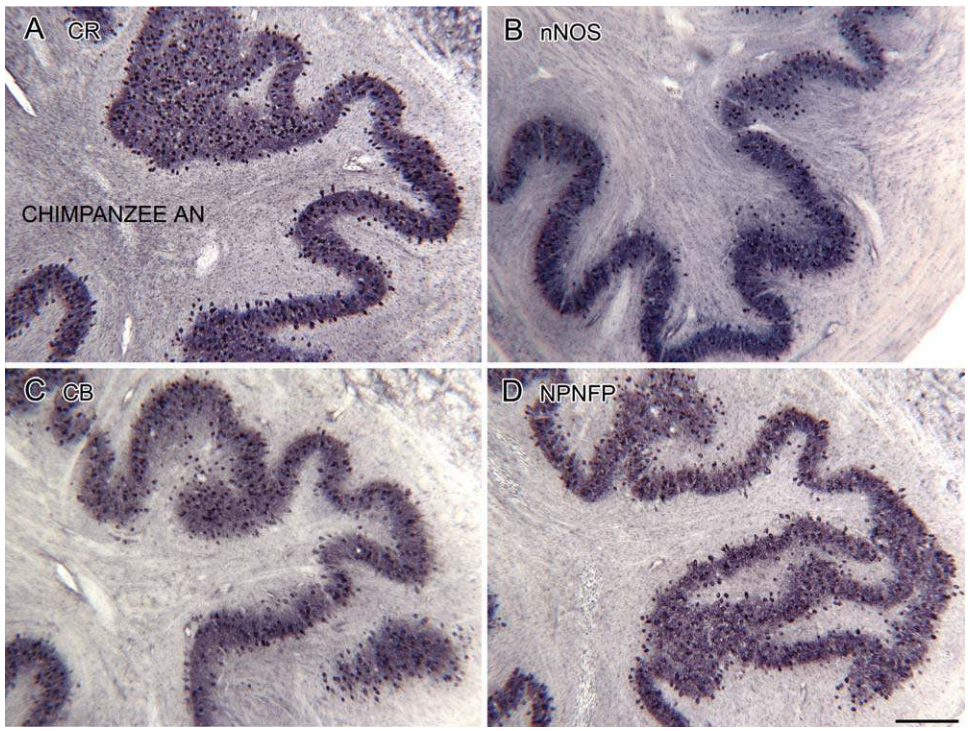

Fig. 14. Expression of CR (**A**), nNOS (**B**), CB (**C**), and NPNFP (**D**) in neurons of the IOpr of chimpanzee AN. Scale bar = 250 μm.

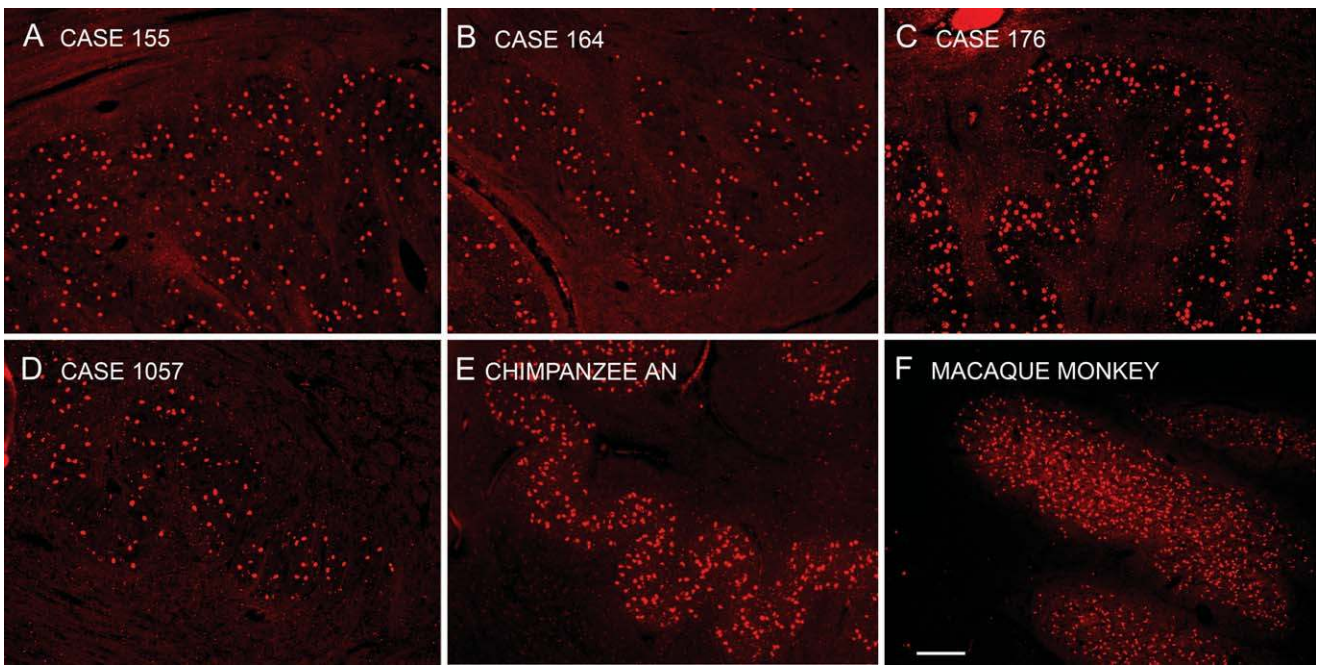

Fig. 15. Autofluorescent neurons in the IOpr of four human cases (**A**) Case 155, age 50; (**B**) Case 164, age 45; (**C**) Case 176, age 71; and (**D**) Case 1057, age 40; (**E**) chimpanzee AN, age 45; and (**F**) macaque monkey, age unknown. Scale bar = 200 μm.

different proteins in any one individual, and at overall different rates among different individuals. This interpretation is consistent with one earlier report showing a decrease in CB expression with age (Nag and Wadhwa, 2004). It would be of great interest to know what determines the rate of lipofuscin accumulation, the relation

TABLE 4. Numbers of figures from three different reports showing immunolabeling in different brainstem structures in cases from the Witelson Normal Brain Collection

Report	Case 155	Case 158	Case 164	Case 168	Case 176	Case 180
IOpr	6D-CR 12A-GAD 15A-LF	7A,B,C-CR 9B-PV 11A-NPNFP 12B-GAD	6C-CR 8C-CB 8D-CB (cbllm) 10A-nNOS 15B-LF	6B-CR 8B-CB	6A-CR 8A-CB 9A-PV 10C,D-nNOS 11B-NPNFP 15C-LF	11C-NPNFP
Vestibular brainstem[a]	15-CR	4,10,11,15-CR	2,4-CR			
PMD[b]			4, nNOS 5-CB 12-nNos	8-NPNFP	7A,B,C-NPNFP	3A,B-CR 4A,B,C-CB 5A,B-PV

CB, calbindin; cbllm, cerebellum; CR, calretinin; GAD, glutamate decarboxylase; LF, lipofuscin; nNOS, nitric oxide synthase; NPNFP, nonhosphorylated neurofilament protein; PV, parvalbumin.
[a]Baizer and Broussard (2010).
[b]Baizer et al. (2007a, 2007b).

between lipofuscin accumulation, and other neurochemical changes including RNA loss, and why some individuals are more vulnerable to this process than others (e.g. Cases 168 and 176 have many more stained neurons than Cases 155 and 164). Further, considering that the chimpanzee and monkey showed both autofluorescence and consistent immunolabel in the IOpr, the relation between pigment accumulation and these other neurochemical changes may be complex and species-specific.

One prediction is that the endpoint of these neurochemical changes is cell death (Mann and Yates, 1974). However, the data on cell loss in the IOpr with age are not consistent. Olszewski and Baxter (1982) noted "these [IO] neurons tend to accumulate lipofuscin very early in life and the Nissl stained section of 'normal' persons over middle age may show a striking paucity of neurons" but did not describe the numbers of cases or present any quantitative analysis. Several studies, using several different methods, have counted the numbers of neurons in the human IOpr (Moatamed, 1966; Escobar et al., 1968; Monagle and Brody, 1974; Pesce et al., 1990; Sjőbeck et al., 1999; Lasn et al., 2001). None saw a consistent decrease in cell number with age, including the one study using stereologic methods (Lasn et al., 2001).

There are several disease processes that are known to result in cell loss in the IOpr, for example Alzheimer's disease (Lasn et al., 2001). This observation is consistent with the finding of NPNFP expression in the IOpr and the link between NPNFP expression and the loss of neurons in the cerebral cortex (Hof et al., 1990; Bussiere et al., 2003). Cerebellar or brainstem damage, specifically to the central tegmental tract, results in a specific type of degeneration in the olive, "hypertrophic olivary degeneration," (Weber, 1942; Gautier and Blackwood, 1961; Goto et al., 1988; Braak et al., 2003; Rüb et al., 2005; Aladdin et al., 2008; Valente et al., 2008). There is also degeneration of IO neurons in several neurological disorders, for example spinocerebellar ataxias and Joubert syndrome (Braak et al., 2003; Rüb et al., 2005; Valente et al., 2008; Popescu et al., 2009).

Functional Implications of Neuronal Changes in the IOpr

Neurons in the IO provide climbing fiber input to the cerebellum; neurochemical changes in IOpr neurons may therefore affect their physiology and hence cerebellar function. The traditional view of the functions of the cerebellum is that it mediates motor control, specifically coordination (Ramnani, 2006; Sultan and Glickstein, 2007). The primate cerebellar hemispheres, the dentate nucleus and the IOpr are especially important in motor control of the hands and fingers (Glickstein et al., 2005, 2009). An alternative view of the cerebellum as important in cognitive function has arisen on the basis of data from imaging, behavioral, and anatomical studies (Middleton and Strick, 1996, 1997, 2000; Dum et al., 2002; Schmahmann, 2004; Teitelbaum et al., 2004; Stoodley and Schmahmann, 2009). It has also been proposed that climbing fiber input is essential for cerebellar plasticity and learning (Gilbert and Thach, 1977; Gibson et al., 2004). The changes of IOpr neurons might then contribute to the age-related decline in executing known motor skills or learning new ones (Spirduso et al., 1988; Woollacott and Shumway-Cook, 2002; Scherder et al., 2008; Fraser et al., 2009) or to a decline in cognitive or language functions mediated by the cerebellum.

ACKNOWLEDGMENTS

Supported in part by the Department of Physiology and Biophysics, University at Buffalo, a grant from the James S. McDonnell Foundation to C.C.S. and P.R.H. and NIH Grant NS42687 to C.C.S. Raquel Lima, Nicolas Paolone, and Vitaly Kramer provided invaluable technical assistance. The authors are grateful to Debra L. Kigar for help in selecting the cases from the Witelson Normal Brain Collection and with the dissections. They thank Alan Gibson for providing images of the sections used to construct the 3D model of the IOpr, and Drs. V. Haroutunian (New York) and C. Bouras (Geneva) for providing some of the human materials used in this study.

LITERATURE CITED

Adams JC. 1981. Heavy metal enhancement of DAB-based HRP reaction product. J Histochem Cytochem 29:775.

Aladdin Y, Scozzafava J, Muayqil T, Saqqur M. 2008. Pearls & oysters: oculopalatal tremor with one-and-a-half syndrome after pontine hemorrhage. Neurology 71:e39–e41.

Amunts K, Schlaug G, Schleicher A, Steinmetz H, Dabringhaus A, Roland PE, Zilles K. 1996. Asymmetry in the human motor cortex and handedness. Neuroimage 4:216–222.

Arai R, Winsky L, Arai M, Jacobowitz DM. 1991. Immunohistochemical localization of calretinin in the rat hindbrain. J Comp Neurol 310:21–44.

Armstrong DM. 1974. Functional significance of connections of the inferior olive. Physiol Rev 54:358–417.

Azizi SA, Woodward DJ. 1987. Inferior olivary nuclear complex of the rat: morphology and comments on the principles of organization within the olivocerebellar system. J Comp Neurol 263:467–484.

Baizer J, Baker J. 2005. Immunoreactivity for calcium-binding proteins defines subregions of the vestibular nuclear complex of the cat. Exp Brain Res 164:78–91.

Baizer J, Lima R, Witelson S, Kigar D, Baker J. 2007a. Neurochemical organization of the inferior olive. In: Neural Control of Movement Annual Meeting, #83. Seville, Spain.

Baizer J, Paolone NA, Witelson SF. 2011. Nonphosphorylated neurofilament protein is expressed by scattered neurons in the human vestibular brainstem. Brain Res 1382:45–56.

Baizer JS, Baker JF. 2006a. Immunoreactivity for calretinin and calbindin in the vestibular nuclear complex of the monkey. Exp Brain Res 172:103–113.

Baizer JS, Baker JF. 2006b. Neurochemically defined cell columns in the nucleus prepositus hypoglossi of the cat and monkey. Brain Res 1094:127–137.

Baizer JS, Baker JF, Haas K, Lima R. 2007b. Neurochemical organization of the nucleus paramedianus dorsalis in the human. Brain Res 1176:45–52.

Baizer JS, Broussard DM. 2010. Expression of calcium-binding proteins and nNOS in the human vestibular and precerebellar brainstem. J Comp Neurol 518:872–895.

Baker J, Lima R, Baizer J. 2007. Neurochemical organization of the inferior olive. Neurosci Abs 512.20/RR24.

Balsters JH, Cussans E, Diedrichsen J, Phillips KA, Preuss TM, Rilling JK, Ramnani N. 2010. Evolution of the cerebellar cortex: the selective expansion of prefrontal-projecting cerebellar lobules. Neuroimage 49:2045–2052.

Barden H. 1970. Relationship of golgi thiaminepyrophosphatase and lysosomal acid phosphatase to neuromelanin and lipofuscin in cerebral neurons of the aging rhesus monkey. J Neuropathol Exp Neurol 29:225–240.

Best AR, Regehr WG. 2009. Inhibitory regulation of electrically coupled neurons in the inferior olive is mediated by asynchronous release of GABA. Neuron 62:555–565.

Braak H, Rüb U, Del Tredici K. 2003. Involvement of precerebellar nuclei in multiple system atrophy. Neuropathol Appl Neurobiol 29:60–76.

Brizzee KR. 1981. Structural correlates of the aging process in the brain. Psychopharmacol Bull 17:43–52.

Brizzee KR, Ordy JM, Kaack B. 1974. Early appearance and regional differences in intraneuronal and extraneuronal lipofuscin accumulation with age in the brain of a nonhuman primate (*Macaca mulatta*). J Gerontol 29:366–381.

Brochu G, Maler L, Hawkes R. 1990. Zebrin II: a polypeptide antigen expressed selectively by Purkinje cells reveals compartments in rat and fish cerebellum. J Comp Neurol 291:538–552.

Brodal A, Walberg F, Blackstad T. 1950. Termination of spinal afferents to inferior olive in cat. J Neurophysiol 13:431–454.

Buffo A, Carulli D, Rossi F, Strata P. 2003. Extrinsic regulation of injury/growth-related gene expression in the inferior olive of the adult rat. Eur J Neurosci 18:2146–2158.

Buffo A, Fronte M, Oestreicher AB, Rossi F. 1998. Degenerative phenomena and reactive modifications of the adult rat inferior olivary neurons following axotomy and disconnection from their targets. Neuroscience 85:587–604.

Bussière T, Giannakopoulos P, Bouras C, Perl DP, Morrison JH, Hof PR. 2003. Progressive degeneration of nonphosphorylated neurofilament protein-enriched pyramidal neurons predicts cognitive impairment in Alzheimer's disease: stereologic analysis of prefrontal cortex area 9. J Comp Neurol 463:281–302.

Carulli D, Buffo A, Strata P. 2004. Reparative mechanisms in the cerebellar cortex. Prog Neurobiol 72:373–398.

Celio MR. 1990. Calbindin D-28k and parvalbumin in the rat nervous system. Neuroscience 35:375–475.

Cunningham DJ. 1903. Text-book of anatomy. New York: W. Wood and Company.

Dayan AD. 1971. Comparative neuropathology of ageing. Studies on the brains of 47 species of vertebrates. Brain 94:31–42.

DeFelipe J. 1999. Chandelier cells and epilepsy. Brain 122:1807–1822.

DeFelipe J. 2002. Cortical interneurons: from Cajal to 2001. Prog Brain Res 136:215–238.

Drach LM, Bohl J, Goebel HH. 1994. The lipofuscin content of nerve cells of the inferior olivary nucleus in Alzheimer's disease. Dementia 5:234–239.

Dum RP, Li C, Strick PL. 2002. Motor and nonmotor domains in the monkey dentate. Ann N Y Acad Sci 978:289–301.

Escobar A, Sampedro ED, Dow RS. 1968. Quantitative data on the inferior olivary nucleus in man, cat and vampire bat. J Comp Neurol 132:397–403.

Floris A, Dino M, Jacobowitz DM, Mugnaini E. 1994. The unipolar brush cells of the rat cerebellar cortex and cochlear nucleus are calretinin-positive: a study by light and electron microscopic immunocytochemistry. Anat Embryol (Berl) 189:495–520.

Fraser SA, Li KZ, Penhune VB. 2009. A comparison of motor skill learning and retention in younger and older adults. Exp Brain Res 195:419–427.

Galaburda AM, Sanides F, Geschwind N. 1978. Human brain. Cytoarchitectonic left–right asymmetries in the temporal speech region. Arch Neurol 35:812–817.

Gautier JC, Blackwood W. 1961. Enlargement of the inferior olivary nucleus in association with lesions of the central tegmental tract or dentate nucleus. Brain 84:341–361.

Geschwind N, Levitsky W. 1968. Human brain: left–right asymmetries in temporal speech region. Science 161:186–187.

Gibson AR, Horn KM, Pong M. 2004. Activation of climbing fibers. Cerebellum 3:212–221.

Gilbert PF, Thach WT. 1977. Purkinje cell activity during motor learning. Brain Res 128:309–328.

Gilligan BC, Shults M, Rhodes RK, Jacobs PG, Brauker JH, Pintar TJ, Updike SJ. 2004. Feasibility of continuous long-term glucose monitoring from a subcutaneous glucose sensor in humans. Diabetes Technol Ther 6:378–386.

Glezer, II, Hof PR, Leranth C, Morgane PJ. 1993. Calcium-binding protein-containing neuronal populations in mammalian visual cortex: a comparative study in whales, insectivores, bats, rodents, and primates. Cereb Cortex 3:249–272.

Glickstein M, Sultan F, Voogd J. 2011. Functional localization in the cerebellum. Cortex 47:59–80.

Glickstein M, Waller J, Baizer JS, Brown B, Timmann D. 2005. Cerebellum lesions and finger use. Cerebellum 4:189–197.

Goto N, Kakimi S, Kaneko M. 1988. Olivary enlargement: stage of initial astrocytic changes. Clin Neuropathol 7:39–43.

Gray DA, Woulfe J. 2005. Lipofuscin and aging: a matter of toxic waste. Sci Aging Knowl Environ 2005:re1.

Gundersen HJ, Bagger P, Bendtsen TF, Evans SM, Korbo L, Marcussen N, Møller A, Nielsen K, Nyengaard JR, Pakkenberg B, Sørensen FB, Vesterby A, West MJ. 1988. The new stereological tools: disector, fractionator, nucleator and point sampled intercepts and their use in pathological research and diagnosis. Acta Pathol Microbiol Immunol Scand 96:857–881.

Gundersen HJ, Jensen EB, Kieu K, Nielsen J. 1999. The efficiency of systematic sampling in stereology—reconsidered. J Microsc 193:199–211.

Hayes TL, Lewis DA. 1992. Nonphosphorylated neurofilament protein and calbindin immunoreactivity in layer III pyramidal neurons of human neocortex. Cereb Cortex 2:56–67.

Hof PR, Cox K, Morrison JH. 1990. Quantitative analysis of a vulnerable subset of pyramidal neurons in Alzheimer's disease: I. Superior frontal and inferior temporal cortex. J Comp Neurol 301:44–54.

Hof PR, Glezer, II, Condé F, Flagg RA, Rubin MB, Nimchinsky EA, Vogt Weisenhorn DM. 1999. Cellular distribution of the calcium-binding proteins parvalbumin, calbindin, and calretinin in the neocortex of mammals: phylogenetic and developmental patterns. J Chem Neuroanat 16:77–116.

Hof PR, Morrison JH. 1991. Neocortical neuronal subpopulations labeled by a monoclonal antibody to calbindin exhibit differential vulnerability in Alzheimer's disease. Exp Neurol 111:293–301.

Hof PR, Morrison JH. 1995. Neurofilament protein defines regional patterns of cortical organization in the macaque monkey visual system: a quantitative immunohistochemical analysis. J Comp Neurol 352:161–186.

Hof PR, Nimchinsky EA, Perl DP, Erwin JM. 2001. An unusual population of pyramidal neurons in the anterior cingulate cortex of hominids contains the calcium-binding protein calretinin. Neurosci Lett 307:139–142.

Hof PR, Ungerleider LG, Adams MM, Webster MJ, Gattass R, Blumberg DM, Morrison JH. 1997. Callosally projecting neurons in the macaque monkey V1/V2 border are enriched in nonphosphorylated neurofilament protein. Vis Neurosci 14:981–987.

Hof PR, Ungerleider LG, Webster MJ, Gattass R, Adams MM, Sailstad CA, Morrison JH. 1996. Neurofilament protein is differentially distributed in subpopulations of corticocortical projection neurons in the macaque monkey visual pathways. J Comp Neurol 376:112–127.

Horn AK, Büttner-Ennever JA. 1998. Premotor neurons for vertical eye movements in the rostral mesencephalon of monkey and human: histologic identification by parvalbumin immunostaining. J Comp Neurol 392:413–427.

Horn AK, Büttner-Ennever JA, Suzuki Y, Henn V. 1995. Histological identification of premotor neurons for horizontal saccades in monkey and man by parvalbumin immunostaining. J Comp Neurol 359:350–363.

Ingham ES, Gunhan E, Fuller PM, Fuller CA. 2009. Immunotoxin-induced ablation of melanopsin retinal ganglion cells in a non-murine mammalian model. J Comp Neurol 516:125–140.

Issidorides M, Shanklin WM. 1961. Histochemical reactions of cellular inclusions in the human neurone. J Anat 95:151–159.

Kondo H, Tanaka K, Hashikawa T, Jones EG. 1999. Neurochemical gradients along monkey sensory cortical pathways: calbindin-immunoreactive pyramidal neurons in layers II and III. Eur J Neurosci 11:4197–4203.

Kooy F. 1917. The inferior olive of vertebrates. Folia Neurobiol 10:205–369.

Lasn H, Winblad B, Bogdanovic N. 2001. The number of neurons in the inferior olivary nucleus in Alzheimer's disease and normal aging: a stereological study using the optical fractionator. J Alzheimers Dis 3:159–168.

Lee VM, Otvos L, Jr., Carden MJ, Hollosi M, Dietzschold B, Lazzarini RA. 1988. Identification of the major multiphosphorylation site in mammalian neurofilaments. Proc Natl Acad Sci USA 85:1998–2002.

MacLeod CE, Zilles K, Schleicher A, Rilling JK, Gibson KR. 2003. Expansion of the neocerebellum in Hominoidea. J Hum Evol 44:401–429.

Mann DM, Yates PO. 1974. Lipoprotein pigments—their relationship to ageing in the human nervous system. I. The lipofuscin content of nerve cells. Brain 97:481–488.

Mann DM, Yates PO, Stamp JE. 1978. The relationship between lipofuscin pigment and ageing in the human nervous system. J Neurol Sci 37:83–93.

Martin GF, Henkel CK, King JS. 1976. Cerebello-olivary fibers: their origin, course and distribution in the North American opossum. Exp Brain Res 24:219–236.

Matano S, Hirasaki E. 1997. Volumetric comparisons in the cerebellar complex of anthropoids, with special reference to locomotor types. Am J Phys Anthropol 103:173–183.

Matano S, Ohta H. 1999. Volumetric comparisons on some nuclei in the cerebellar complex of prosimians. Am J Primatol 48:31–48.

Middleton FA, Strick PL. 1996. Basal ganglia and cerebellar output influences non-motor function. Mol Psychiatry 1:429–433.

Middleton FA, Strick PL. 1997. Dentate output channels: motor and cognitive components. Prog Brain Res 114:553–566.

Middleton FA, Strick PL. 2000. Basal ganglia and cerebellar loops: motor and cognitive circuits. Brain Res Brain Res Rev 31:236–250.

Milosevic A, Zecevic N. 1998. Developmental changes in human cerebellum: expression of intracellular calcium receptors, calcium-binding proteins, and phosphorylated and nonphosphorylated neurofilament protein. J Comp Neurol 396:442–460.

Moatamed F. 1966. Cell frequencies in the human inferior olivary nuclear complex. J Comp Neurol 128:109–116.

Monagle RD, Brody H. 1974. The effects of age upon the main nucleus of the inferior olive in the human. J Comp Neurol 155:61–66.

Moreno-López B, Escudero M, De Vente J, Estrada C. 2001. Morphological identification of nitric oxide sources and targets in the cat oculomotor system. J Comp Neurol 435:311–324.

Nag TC, Wadhwa S. 2004. Ontogeny of two calcium-binding proteins (calbindin D-28K and parvalbumin) in the human inferior olivary complex and their distribution in the adults. J Chem Neuroanat 27:183–192.

Nunzi MG, Shigemoto R, Mugnaini E. 2002. Differential expression of calretinin and metabotropic glutamate receptor mGluR1alpha defines subsets of unipolar brush cells in mouse cerebellum. J Comp Neurol 451:189–199.

Olszewski J, Baxter D. 1982. Cytoarchitecture of the human brain stem. 2nd ed. Basel: Karger.

Paxinos G, Carrive P, Wang H, Wang P-Y. 1999. Chemoarchitectonic atlas of the rat brainstem. San Diego: Academic Press.

Paxinos G, Franklin KBJ. 2001. The mouse brain in stereotaxic coordinates. 2nd ed. San Diego: Academic Press.

Paxinos G, Huang XF. 1995. Atlas of the human brainstem. San Diego: Academic Press.

Paxinos G, Törk I, Halliday G, Mehler W. 1990. Human homologs to brainstem nuclei identified in other animals as revealed by acetylcholinesterase activity. In: Paxinos G, editor. The human nervous system. San Diego: Academic Press. p 149–202.

Pesce C, Provera P, Dessanti P, Provaggi MA. 1990. Densitometric analysis of the nerve cell population of the inferior olive in aging. Acta Neuropathol 80:95–97.

Popescu BF, Robinson CA, Chapman LD, Nichol H. 2009. Synchrotron X-ray fluorescence reveals abnormal metal distributions in brain and spinal cord in spinocerebellar ataxia: a case report. Cerebellum 8:340–351.

Rakic P. 1995. A small step for the cell, a giant leap for mankind: a hypothesis of neocortical expansion during evolution. Trends Neurosci 18:383–388.

Ramnani N. 2006. The primate cortico-cerebellar system: anatomy and function. Nat Rev Neurosci 7:511–522.

Résibois A, Rogers JH. 1992. Calretinin in rat brain: an immunohistochemical study. Neuroscience 46:101–134.

Rodrigo J, Springall DR, Uttenthal O, Bentura ML, Abadia-Molina F, Riveros-Moreno V, Martinez-Murillo R, Polak JM, Moncada S. 1994. Localization of nitric oxide synthase in the adult rat brain. Philos Trans R Soc Lond B: Biol Sci 345:175–221.

Rogers JH, Résibois A. 1992. Calretinin and calbindin-D28k in rat brain: patterns of partial co-localization. Neuroscience 51:843–865.

Rüb U, Gierga K, Brunt ER, de Vos RA, Bauer M, Schols L, Burk K, Auburger G, Bohl J, Schultz C, Vuksic M, Burbach GJ, Braak H, Deller T. 2005. Spinocerebellar ataxias types 2 and 3: degeneration of the pre-cerebellar nuclei isolates the three phylogenetically defined regions of the cerebellum. J Neural Transm 112: 1523–1545.

Scherder E, Dekker W, Eggermont L. 2008. Higher-level hand motor function in aging and (preclinical) dementia: its relationship with (instrumental) activities of daily life—a mini-review. Gerontology 54:333–341.

Schmahmann JD. 2004. Disorders of the cerebellum: ataxia, dysmetria of thought, and the cerebellar cognitive affective syndrome. J Neuropsychiatry Clin Neurosci 16:367–378.

Schnell SA, Staines WA, Wessendorf MW. 1999. Reduction of lipofuscin-like autofluorescence in fluorescently labeled tissue. J Histochem Cytochem 47:719–730.

Sherwood CC, Hof PR, Holloway RL, Semendeferi K, Gannon PJ, Frahm HD, Zilles K. 2005. Evolution of the brainstem orofacial motor system in primates: a comparative study of trigeminal, facial, and hypoglossal nuclei. J Hum Evol 48:45–84.

Sherwood CC, Subiaul F, Zawidzki TW. 2008. A natural history of the human mind: tracing evolutionary changes in brain and cognition. J Anat 212:426–454.

Sjőbeck M, Dahlén S, Englund E. 1999. Neuronal loss in the brainstem and cerebellum—part of the normal aging process? A morphometric study of the vermis cerebelli and inferior olivary nucleus. J Gerontol A: Biol Sci Med Sci 54:B363–B368.

Spirduso WW, MacRae HH, MacRae PG, Prewitt J, Osborne L. 1988. Exercise effects on aged motor function. Ann N Y Acad Sci 515:363–375.

Sternberger LA, Sternberger NH. 1983. Monoclonal antibodies distinguish phosphorylated and nonphosphorylated forms of neurofilaments in situ. Proc Natl Acad Sci USA 80:6126–6130.

Stoodley CJ, Schmahmann JD. 2009. The cerebellum and language: evidence from patients with cerebellar degeneration. Brain Lang 110:149–153.

Sultan F, Glickstein M. 2007. The cerebellum: comparative and animal studies. Cerebellum 6:168–176.

Sultan F, Hamodeh S, Baizer JS. 2010. The human dentate nucleus: a complex shape untangled. Neuroscience 167:965–968.

Teitelbaum O, Benton T, Shah PK, Prince A, Kelly JL, Teitelbaum P. 2004. Eshkol-Wachman movement notation in diagnosis: the early detection of Asperger's syndrome. Proc Natl Acad Sci USA 101:11909–11914.

Terman A, Brunk UT. 2004. Lipofuscin. Int J Biochem Cell Biol 36:1400–1404.

Toga AW, Thompson PM. 2003. Mapping brain asymmetry. Nat Rev Neurosci 4:37–48.

Valente EM, Brancati F, Dallapiccola B. 2008. Genotypes and phenotypes of Joubert syndrome and related disorders. Eur J Med Genet 51:1–23.

Van Brederode JF, Mulligan KA, Hendrickson AE. 1990. Calcium-binding proteins as markers for subpopulations of GABAergic neurons in monkey striate cortex. J Comp Neurol 298:1–22.

Van der Gucht E, Youakim M, Arckens L, Hof PR, Baizer JS. 2006. Variations in the structure of the prelunate gyrus in Old World monkeys. Anat Rec 288:753–775.

Voogd J, Feirabend H, Schoen J. 1990. Cerebellum and precerebellar nuclei. In: Paxinos G, editor. The human nervous system. San Diego: Academic Press.

Wada JA, Clarke R, Hamm A. 1975. Cerebral hemispheric asymmetry in humans. Cortical speech zones in 100 adults and 100 infant brains. Arch Neurol 32:239–246.

Wassef M, Chédotal A, Cholley B, Thomasset M, Heizmann CW, Sotelo C. 1992. Development of the olivocerebellar projection in the rat: I. Transient biochemical compartmentation of the inferior olive. J Comp Neurol 323:519–536.

Weber FP. 1942. Cerebello-olivary degeneration: an example of heredo-familial incidence. Brain 65:220–231.

Witelson SF, McCulloch PB. 1991. Premortem and postmortem measurement to study structure with function: a human brain collection. Schizophr Bull 17:583–591.

Woollacott M, Shumway-Cook A. 2002. Attention and the control of posture and gait: a review of an emerging area of research. Gait Posture 16:1–14.

Yu MC, Cho E, Luo CB, Li WW, Shen WZ, Yew DT. 1996. Immunohistochemical studies of GABA and parvalbumin in the developing human cerebellum. Neuroscience 70:267–276.